frontiers | Frontiers in Marine Science

TYPE Original Research
PUBLISHED 12 May 2023
DOI 10.3389/fmars.2023.1082077

OPEN ACCESS

EDITED BY
Ilana Berman-Frank,
University of Haifa, Israel

REVIEWED BY
Ruifeng Zhang,
Shanghai Jiao Tong University, China
Zhibing Jiang,
Ministry of Natural Resources, China

*CORRESPONDENCE
Chloé Tilliette
chloe.tilliette@imev-mer.fr
Frédéric Gazeau
frederic.gazeau@imev-mer.fr
Cécile Guieu
cecile.guieu@imev-mer.fr

RECEIVED 27 October 2022
ACCEPTED 22 March 2023
PUBLISHED 12 May 2023

CITATION
Tilliette C, Gazeau F, Portlock G, Benavides M, Bonnet S, Guigue C, Leblond N, Lory C, Marie D, Montanes M, Pulido-Villena E, Sarthou G, Tedetti M, Vorrath M-E, Whitby H and Guieu C (2023) Influence of shallow hydrothermal fluid release on the functioning of phytoplankton communities. *Front. Mar. Sci.* 10:1082077. doi: 10.3389/fmars.2023.1082077

Influence of shallow hydrothermal fluid release on the functioning of phytoplankton communities

Chloé Tilliette[1*], Frédéric Gazeau[1*], Gemma Portlock[2], Mar Benavides[3], Sophie Bonnet[3], Catherine Guigue[3], Nathalie Leblond[1], Caroline Lory[3], Dominique Marie[4], Maryline Montanes[1], Elvira Pulido-Villena[3], Géraldine Sarthou[5], Marc Tedetti[3], Maria-Elena Vorrath[6], Hannah Whitby[2] and Cécile Guieu[1*]

[1]Sorbonne Université, CNRS, Laboratoire d'Océanographie de Villefranche, LOV, Villefranche-sur-Mer, France, [2]Department of Earth, Ocean and Ecological Sciences, School of Environmental Sciences, University of Liverpool, Liverpool, United Kingdom, [3]Aix Marseille Univ., Université de Toulon, CNRS, IRD, MIO, Marseille, France, [4]CNRS, Sorbonne Université, UMR7144, Team ECOMAP, Station Biologique de Roscoff, Roscoff, France, [5]University of Brest, CNRS, IRD, Ifremer, LEMAR, Plouzané, France, [6]Intitut für Geologie, University Hamburg, Hamburg, Germany

In the Western Tropical South Pacific (WTSP) Ocean, a hotspot of dinitrogen fixation has been identified. The survival of diazotrophs depends, among others, on the availability of dissolved iron (DFe) largely originating, as recently revealed, from shallow hydrothermal sources located along the Tonga-Kermadec arc that fertilize the Lau Basin with this element. On the opposite, these fluids, released directly close to the photic layer, can introduce numerous trace metals at concentrations that can be toxic to surface communities. Here, we performed an innovative 9-day experiment in 300 L reactors onboard the TONGA expedition, to examine the effects of hydrothermal fluids on natural plankton communities in the WTSP Ocean. Different volumes of fluids were mixed with non-hydrothermally influenced surface waters (mixing ratio from 0 to 14.5%) and the response of the communities was studied by monitoring numerous stocks and fluxes (phytoplankton biomass, community composition, net community production, N_2 fixation, thiol production, organic carbon and metal concentrations in exported material). Despite an initial toxic effect of hydrothermal fluids on phytoplankton communities, these inputs led to higher net community production and N_2 fixation rates, as well as elevated export of organic matter relative to control. This fertilizing effect was achieved through detoxification of the environment, rich in potentially toxic elements (e.g., Cu, Cd, Hg), likely by resistant *Synechococcus* ecotypes able to produce strong binding ligands, especially thiols (thioacetamide-like and glutathione-like compounds). The striking increase of thiols quickly after fluid addition likely detoxified the environment, rendering it more favorable for phytoplankton growth. Indeed, phytoplankton groups stressed by the addition of fluids were then able to recover important growth rates, probably favored by the supply of numerous fertilizing trace metals (notably Fe) from hydrothermal fluids and new nitrogen provided by N_2 fixation. These experimental results are in good agreement with *in-situ*

observations, proving the causal link between the supply of hydrothermal fluids emitted at shallow depth into the surface layer and the intense biological productivity largely supported by diazotrophs in the WTSP Ocean. This study highlights the importance of considering shallow hydrothermal systems for a better understanding of the biological carbon pump.

KEYWORDS

hydrothermal fluids, phytoplankton communities, trace metal, fertilizing effect, toxic effect, Western Tropical South Pacific, community functioning, thiol compounds

1 Introduction

The Western Tropical South Pacific (WTSP) Ocean (18-22°S, 160°E-160°W) has recently been recognized as a hotspot of dinitrogen (N_2) fixation, harboring some of the highest rates reported to date in the global ocean (Bonnet et al., 2017). Diazotrophs (i.e., N_2-fixing organisms) have high cellular iron (Fe) quotas relative to other plankton functional groups, as Fe is an essential component of the nitrogenase enzyme catalyzing N_2 fixation (Rueter et al., 1992; Berman-Frank et al., 2001). Hence, their biogeographical distribution has been closely related to ambient Fe concentrations, especially in the subtropical Atlantic Ocean and the WTSP Ocean (Schlosser et al., 2014; Lory et al., 2022). In the WTSP Ocean, diazotroph blooms have also been attributed to elevated, non-limiting concentrations of Fe, along with optimal conditions of temperature and phosphorus availability (Moutin et al., 2005; Moutin et al., 2008). Prior to the OUTPACE (Moutin and Bonnet, 2015) and TONGA (Guieu and Bonnet, 2019) cruises performed in the WTSP Ocean, our knowledge of the origin and distribution of Fe in the region was poor, as the Pacific Ocean is severely undersampled, especially for trace metals (Schlitzer et al., 2018). Accurate quantification of dissolved Fe (DFe) distribution along a 6000-km transect during the TONGA cruise has demonstrated that shallow hydrothermal sources (200-300 m) located along the Tonga-Kermadec arc accounted for these elevated DFe concentrations measured in the Lau Basin and Melanesian waters (Tilliette et al., 2022) and trigger the high N_2 fixation rates measured in the region (Bonnet et al., in rev.).

The Tonga-Kermadec subduction zone belongs to the Pacific Ring of Fire hosting nearly three-quarters of the world's active volcanoes (Rinard Hinga, 2015). It is the most linear, convergent and seismically active of the Earth's subduction boundaries (Timm et al., 2013) and consequently carries intense volcanic and hydrothermal activities (2.6 active vents/100 km; Pelletier et al., 1998; Massoth et al., 2007). Submarine hydrothermal activity occurs when water percolates through the fractured oceanic crust. As it penetrates downward, the water is heated (> 400°C) and undergoes chemical changes by reacting with nearby rocks. At this temperature, the fluid becomes buoyant and rises rapidly in the water column (German et al., 2016). Numerous chemical species can be introduced into the water column by hydrothermal plumes at concentrations much higher than those usually found in the water column (Dick et al., 2013; Lilley et al., 2013; González-Vega et al., 2020). These include gases (e.g., carbon dioxide: CO_2, hydrogen sulfide: H_2S, dihydrogen: H_2, helium: He) and macronutrients (e.g., nitrate: NO_3^- , silicate: Si(OH)4, phosphate: PO_4^{3-}). They also contain dissolved and particulate trace metals, some being essential although toxic at high concentrations (e.g., copper: Cu, zinc: Zn) and others non-essential and even harmful (e.g., cadmium: Cd, mercury: Hg, lead: Pb) for many organisms including phytoplankton (Thomas et al., 1980; DalCorso, 2012; Mehana, 2014; Azeh Engwa et al., 2019). Contrary to mid-ocean ridges where hydrothermal vents are located deep (3000-4000 m), in some regions such as the WTSP or the Aegean Sea, hydrothermal vents can be shallow (< 300 m) and inject such elements directly into the surface layer (Massoth et al., 2007; Zhang et al., 2020). Thus, besides fertilization by trace metals such as Fe (Ardyna et al., 2019; Schine et al., 2021), toxic effects may also occur for plankton communities due to the proximity of the vent, where fluids can be highly concentrated in these elements (Lilley et al., 2013). In addition, plumes from shallow hydrothermal sources supply fresher and more labile material (Hawkes et al., 2014) compared to inputs reaching surface waters from deep systems (Tagliabue et al., 2010) and thus may be more bioavailable to surface phytoplankton. These fluids could therefore affect (positively or adversely) the functioning of the planktonic ecosystem and the biological carbon pump.

Numerous studies have reported on the effects of trace metal additions, alone or in combination, in mono-specific cultures or on natural phytoplankton assemblages. They all revealed that plankton communities release binding ligands into the environment to face metal stress (e.g., Lage et al., 1996; Leal et al., 1999; Morel and Price, 2003; Dupont and Ahner, 2005; Horvatić and Peršić, 2007; Hoffmann et al., 2012; Wu and Wang, 2012; Permana and Akbarsyah, 2021). In particular, thiols, which are low molecular weight peptides comprising a sulfhydryl group (–SH; Buckberry and Teesdale-Spittle, 1996; Morrison et al., 2010), are an important component of the ligand pool and have been shown to be responsible for the near-complete complexation of several trace metals in surface waters, rendering them non-bioavailable (Satoh et al., 1999; Tang et al., 2000; Dupont et al., 2006). Such compounds may have a key role in detoxifying an environment rich in harmful elements (Grill et al., 1989; Ahner and Morel, 1995; Zenk, 1996). Yet to date, no study has explored the effect of natural metal-rich

shallow hydrothermal inputs on plankton communities. In the present study, we conducted an innovative experiment to investigate the effects of hydrothermal fluids from shallow sources located along the Tonga-Kermadec arc on natural plankton communities of the WTSP Ocean. During the TONGA cruise, different volumes of hydrothermal fluids collected from an identified active vent along the Tonga arc were added to surface waters collected in a remote area unaffected by hydrothermal fluids. This nine-day experiment allowed for the examination of the community functioning as a whole and for the investigation of the effects of hydrothermal fluids on numerous biological and biogeochemical stocks and fluxes (e.g., biomass, community composition, thiols and fluorescent dissolved organic matter (FDOM) concentrations, biological productivity, N_2 fixation, export of material) in a system mimicking the natural physico-chemical conditions prevailing in the region.

2 Materials and methods

2.1 Hydrothermal fluid enrichment experiment

2.1.1 Experimental design

The experiment was conducted as part of the TONGA cruise (GEOTRACES GPpr14, November 2019, R/V *L'Atalante*; Guieu and Bonnet, 2019) in 300 L high-density polyethylene (HDPE) and trace metal free experimental tanks (referred hereafter as minicosms; Figure 1A). Each minicosm was equipped with a lid supporting six rows of LEDs (Alpheus©) composed of blue, green, cyan and white units mimicking the natural light spectrum. A 250 mL HDPE bottle was screwed onto a polyvinyl chloride valve that remained open throughout the experiment to collect exported material at the conical base of each minicosm. Photosynthetically active radiation (PAR; 400-700 nm) and temperature were continuously monitored in each minicosm using a QSL-2100 irradiance sensor (Biospherical Instruments Inc©) and a HOBO TidbiT® v2 temperature data logger (Onset), respectively.

The experimental system was composed of nine minicosms installed in a light-isolated, air-conditioned, clean-room container (99.9% filtration of particles larger than 0.2 µm by a high efficiency particulate air filter; Figure 1B). Prior to the experiment, minicosms were meticulously washed with a high-pressure cleaner (Kärcher®) and filled with a mixture of fresh water and surfactant (Decon™) for 24 h. They were then refilled with fresh water and acidified with hydrochloric acid (Suprapure HCl; Supelco®; final pH ~2). After 24 h, minicosms were emptied and rinsed with deionized water. The temperature of the container was adjusted 2°C below *in-situ* temperature level to facilitate maintaining temperature close to the targeted level (i.e., *in-situ* temperature) using a temperature-control system placed in each minicosm during the experiment (see thereafter).

The experimental protocol followed a gradient approach, with one control and seven minicosms enriched with increasing volumes of hydrothermal fluids: from 1.8 to 14.5% of the total volume added to surface waters (Table 1). These ratios were chosen based on previous DFe measurements during the OUTPACE cruise (Guieu et al., 2018), where DFe likely from hydrothermal origin reached concentrations up to 66 nM while in surface waters (< 100 m) impacted by these fluids, [DFe] reached 1-2 nM. Depending on their vertical and horizontal distance from the source, communities will be subjected to different fluid-water mixing. Closer to the source, communities will be subjected to higher enrichments (5-12 nM at 100-150 m during OUTPACE, corresponding to mixing rates of 8-18%) while those more distal from the source will be subjected to lower mixing, due to high fluid dilution, similar to those observed at the surface during OUTPACE (corresponding to mixing of 1.5-4.5%). The gradient chosen thus covers the different conditions to which communities may be subjected. The ninth minicosm, labeled M9, was used to sample both end-members (hydrothermal fluids and surface waters unaffected by hydrothermal fluids) for all parameters and processes considered prior to their mixing (see Section 2.1.2).

2.1.2 End-member sampling and mixing protocol

The nine minicosms were first filled with surface water sampled on November 10, 2019, at the western boundary of the South Pacific Gyre (21.69°S, 174.74°W), located outside the influence of volcanic activity and characterized by low chlorophyll concentrations (< 0.1 mg m^{-3}; Figure 1C). Seawater was pumped at 5 m at 10 p.m. (local time) using a high flow peristaltic pump (TecamySer®). A volume of 275 L was evenly and synchronously distributed in the nine minicosms using nine HDPE pipes. M9 was sampled the next day at 6 a.m. for the measurement of all stocks and fluxes, which are necessary to characterize the properties of the surface end-member shortly before mixing. M9 was then emptied and rinsed with deionized water.

Hydrothermal fluids were sampled upon arrival at the station, on November 11, 2019, at 9:30 a.m. (local time). Sampling was performed at 21.15°S, 174.75°W above an active shallow hydrothermal source (Figure 1C). Seawater was pumped at 200 m (i.e., the depth at which the strongest acoustic and chemical anomalies were measured; Tilliette et al., 2022) to fill the minicosm M9 using the same pumping device as for the surface end-member. After having collected the samples for the parameters and processes needed to characterize the fluid end-member, M9 was used for the mixing. In each of the eight minicosms, different volumes of surface seawater were removed and replaced by the same volumes of fluid end-member, following the gradient approach described in Table 1. The entire process (pumping and mixing of the two end-members) required 13 h. Concurrently, a CTD cast (conductivity, temperature and depth; SeaBird SBE 911 Plus rosette-mounted) was performed above the hydrothermal source to compare parameters measured in the minicosms to the *in-situ* data (see below).

2.1.3 Final adjustments and launch of the experiment

Immediately after mixing, 260 mg of ^{13}C-labeled sodium bicarbonate (^{13}C-$NaHCO_3$; Sigma-Aldrich®) was added to each minicosm to monitor the incorporation of dissolved inorganic

10.3389/fmars.2023.1082077

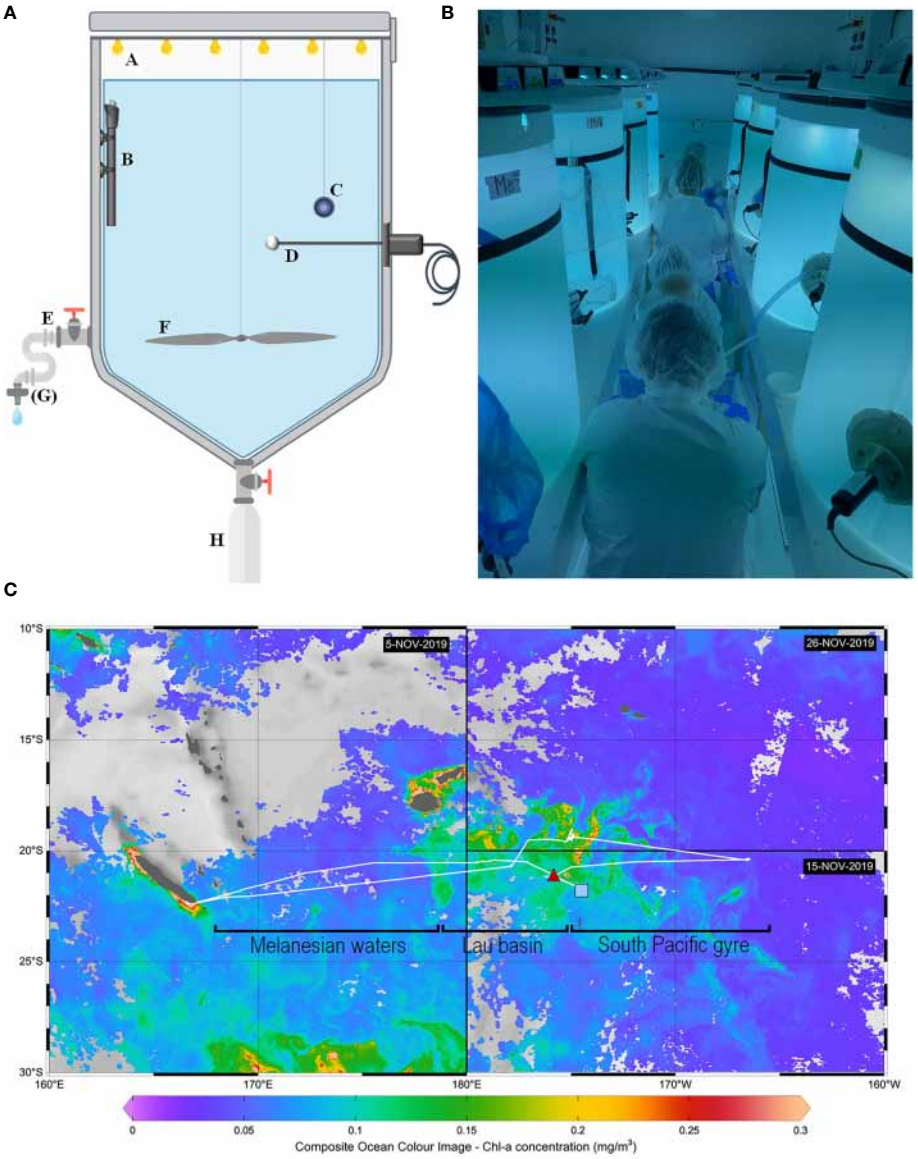

FIGURE 1
Methods used for the hydrothermal fluid enrichment experiment. **(A)** Scheme illustrating the different components of a minicosm with A LED cover, B heating resistor, C temperature data logger, D photosynthetically active radiation (PAR) sensor, E sampling tube, F motorized propeller, G filtration cartridge (used only for some parameters) and H particle trap. **(B)** Picture taken during sampling, showing eight of the nine minicosms used during the experiment and installed in the "clean-room" container. **(C)** Cruise transect superimposed on surface chlorophyll-*a* concentrations (mg m^{-3}). Chlorophyll-*a* concentrations were derived from satellite images acquired during the respective period of occupancy: 5 November 2019 for the western part of the transect, 15 November for the southeastern part, and 29 November for the northeastern part. The position of the end-members sampled for the minicosm experiment is represented by a red triangle for the fluid end-member and a blue square for the surface end-member. Note that an effort was made to sample waters relatively low in chlorophyll-*a* for the surface end-member (< 0.1 mg m^{-3}). The hooks under the transect represent the different subregions studied during the cruise: Melanesian waters and the Lau Basin at the west and the South Pacific Gyre at the east.

TABLE 1 Gradient approach considered for the mixing experiment between surface water and hydrothermal fluids.

Treatment	Control	1.8%	3.6%	5.5%	7.3%	9.1%	10.9%	14.5%
Volume of fluid (L)	0	5	10	15	20	25	30	40
Volume of surface water (L)	275	270	265	260	255	250	245	235

Treatment (in %) represents the proportion of hydrothermal fluid added to surface waters.

carbon (DIC) into particulate organic carbon (POC). An initial ^{13}C-DIC signature of ca. 500‰ was achieved. The rotating propellers fitted in each minicom (Figure 1A) were set at 9 rotations per minute, creating a slight turbulence allowing particles to remain in suspension. A 12:12 light cycle was simulated with a maximum irradiance of ~735 µmol photons m^{-2} s^{-1} reached between 9:30 a.m. and 5 p.m. (local time). The seawater temperature in each minicosm was regulated during the entire experiment to the surface *in-situ* value (25.7°C) using heating resistors (500 W; Aquamedic™) regulated by control units (Corema™).

2.1.4 Sampling

Sampling was performed on six occasions for most parameters during the nine-day experiment: 12 h (day 0.5), 24 h (day 1), 48 h (day 2), 96 h (day 4), 144 h (day 6) and 216 h (day 9) after mixing the two end-members. However, some parameters requiring low volume, such as for flow cytometry analyses, were sampled daily. The parameters studied included: photosynthetic pigment concentrations, phytoplankton abundances, net community production (NCP), N_2 fixation rates, DFe, thiols, FDOM and nutrients concentrations. All samples were collected from the sampling tube installed on each minicosm (Figure 1A) under the cleanest possible conditions by gravity and without filtration, except for thiol and macronutrient samples filtered on sterile Sartobran® 300 cartridges (0.45 µm pre-filtration and 0.2 µm final filtration) connected to the sampling tubes of each tank. Macro-nutrients were analyzed (see Text S1) and are described in detail in Bonnet et al. (in rev.). The sampling protocol is illustrated in Table S1. The duration of the experiment was imposed by the tight schedule of the cruise and the need to sample less than 50% of the initial volume by the end of the experiment to minimize the associated bias.

2.2 Analytical methods

2.2.1 Dissolved iron and particulate trace metals

DFe samples were collected in 60 mL LDPE bottles after filtration through sterile Sartobran® 300 cartridges (pre-filtration on 0.45 µm and final filtration on 0.2 µm). Right after collection, seawater samples were acidified to pH ~1.7 with 2‰ (v/v) hydrochloric acid (HCl, Ultrapure® Merck) under a class 100 laminar flow hood, double-bagged, and stored at ambient temperature in the dark before shore-based analysis. DFe concentrations were determined by flow injection and chemiluminescence detection as described in Tilliette et al. (2022).

Trace-metal clean rosette casts were conducted to sample dissolved and particulate trace metals above the hydrothermal source. DFe samples were analyzed as described above (see Tilliette et al. (2022) for further details). The protocol for other dissolved and particulate trace metal measurements is presented in Text S2.

2.2.2 Biological stocks

2.2.2.1 Photosynthetic pigments

Samples of 2.7 L were filtered within 2 h of collection through 25 mm glass fiber filters (GF/F; Whatman™; 0.7 µm). After filtration, filters were transferred to cryovials, flash-frozen in liquid nitrogen and stored at -80°C pending analysis. Nine months after collection, samples were processed by the SAPIGH analytical platform at the Institut de la Mer de Villefranche (IMEV, France). Filters were extracted at -20°C in 3 mL of methanol (100%) containing vitamin E acetate (Sigma-Aldrich®). They were crushed by sonication before being clarified one hour later by vacuum filtration. The extracts were analyzed within 24 h using a complete Agilent Technologies® 1200 series high-performance liquid chromatography (HPLC) system. The contribution of the identified pigments and their taxonomic significance were determined according to Uitz et al. (2006). The biomass of haptophyceae, diatoms and dinoflagellates was thus estimated from 19'-hexanoyloxyfucoxanthin, fucoxanthin and peridinin, respectively.

2.2.2.2 Abundance of Synechococcus and Prochlorococcus cells

Samples of 7 mL were fixed with a mixture of 0.25% glutaraldehyde and 0.01% Pluronic F-68, flash-frozen in liquid nitrogen and stored at -80°C pending analysis. Samples were analyzed at the Station Biologique de Roscoff as described in Marie et al. (1999). Briefly, 1 mL of thawed sample was transferred into a cryotube and analyzed using a BD FACSCanto™ II flow cytometer equipped with 488 and 633 nm lasers. Signal was triggered on red fluorescence and samples were run for 3 minutes with a flow rate around 100 µL min^{-1}. *Synechococcus* were discriminated from *Prochlorococcus* cells through the presence of the pigment phycoerythrin.

During the cruise, rosette casts were conducted to sample for photosynthetic pigments as well as *Prochlorococcus* and *Synechococcus* abundances above the hydrothermal source. The collected samples were analyzed as described above.

2.2.3 Biological fluxes

2.2.3.1 Net community production

Samples of 2.7 L were filtered through pre-combusted (450°C, 4 h) and pre-weighed GF/F filters. Filters were then stored in petri dishes and dried at 60°C for 24 h. Shortly before analysis, each sample was acidified by adding HCl (2 N) to remove the inorganic carbon fraction. POC concentrations and carbon isotopic signature were measured by an elemental analyzer coupled to an isotope ratio mass spectrometer (EA-IRMS; Vario Pyrocube-Isoprime 100, Elementar®). DIC concentrations were determined using the R package *seacarb* developed by Lavigne and Gattuso (2010) using the pre-requisite pH and total alkalinity data measured during the experiment (see Texts S3, S4). δ^{13}C-DIC concentrations were measured as described in Maugendre et al. (2017). NCP was finally calculated using all these parameters according to the method of de Kluijver et al. (2010).

2.2.3.2 N_2 fixation rates

Rates were measured using the $^{15}N_2$ bubble technique (Montoya et al., 1996), intentionally chosen to avoid any potential trace metal or dissolved organic matter contaminations (Klawonn et al., 2015), as both have been found to control N_2 fixation or *nifH* gene expression in

this region (Moisander et al., 2014; Benavides et al., 2017). Samples collected in 2.25 L acid-washed polycarbonate bottles were amended with 2 mL of 98.9% $^{15}N_2$ (Cambridge isotopes), incubated in on-deck incubators connected to surface circulating seawater and shaded at the specified irradiances using blue screening. Incubations were stopped by filtering the entire incubation bottle onto pre-combusted (450°C, 4 h) GF/F filters. Filters were subsequently dried at 60°C for 24 h before analysis of ^{15}N:^{14}N ratio and particulate N using an EA-IRMS (Integra 2, SerCon Ltd) as described in Bonnet et al. (2018). The^{15}N:^{14}N of the N_2 pool available for N_2 fixation (Montoya et al., 1996) was measured in all incubation bottles by membrane inlet mass spectrometry to ensure accurate rate calculations as fully described in Bonnet et al. (2018).

2.2.4 Dissolved organic compounds

2.2.4.1 Thiols

Thiol samples were collected in 125 mL trace metal-clean low-density polyethylene (LDPE) bottles (Nalgene®) after filtration through sterile Sartobran® 300 cartridges. Samples were then double-bagged and stored frozen at -20°C pending analysis. Samples were defrosted at room temperature in the dark, and thiol concentrations were measured electrochemically using a Metrohm μAutolab III. The working electrode was a hanging mercury drop electrode, the reference electrode was Ag/AgCl with a glass salt bridge filled with 3 M KCl, and the counter electrode a glassy carbon rod. The voltammetric method was taken from Pernet-Coudrier et al. (2013).

Briefly, a sample aliquot of 10 mL was transferred into an acid-cleaned voltammetric quartz cell under a laminar flow hood and acidified to pH 2 using trace-metal grade HCl. The solution was spiked with 30 μL of 10 ppm molybdenum(VI) and then purged with nitrogen (99.99%) for 5 minutes. A deposition potential of 0 V was applied for 150 s with stirring followed by a 5-s rest time. Using differential pulse mode, the potential scan ranged from 0 to -0.65 V. Compound concentrations were determined by standard addition of thioacetamide (TA, Fisher Scientific) and glutathione (GSH, reduced, Sigma-Aldrich) standards. Two additions were made for each sample, with four measurements per addition. The peak height was measured using ECDSOFT (Omanović and Branica, 1998).

2.2.4.2 Fluorescent dissolved organic matter

FDOM samples were collected in pre-calcined glass bottles and immediately filtered through pre-calcined GF/F filters using a low vacuum glass filtration system. The resulting filtrates were transferred to 100 mL pre-calcined amber glass bottles with Teflon®-lined caps. The ampoules were stored in the dark at -20°C until analysis.

Within three months of collection, FDOM measurements were performed with a F-7000 spectrofluorometer (Hitachi®). Excitation-emission matrices (EEMs) were conducted over the excitation (λ_{Ex}) and emission (λ_{Em}) wavelength ranges of 200-500 nm and 280-550 nm, respectively. EEMs were blank-corrected, Raman-normalized and converted into quinine sulfate unit (QSU). EEMs were treated with parallel factor analysis (PARAFAC) executed using the DOMFluortoolbox v1.6 (Stedmon and Bro, 2008) running under MATLAB® 7.10.0 (R2010a) for the identification of the main fluorophores according to Ferretto et al. (2017) and Tedetti et al. (2016); Tedetti et al. (2020).

2.2.5 Exported material

At the end of the experiment, particle traps were removed, closed and stored at 4°C in the dark in a 4% formaldehyde solution pending analysis. Samples were processed according to the standard protocol followed by the "Cellule Pièges" (INSU-CNRS). After removal of the swimmers (zooplankton), samples were rinsed three times in MilliQ water and lyophilized. The total amount of material collected was weighed to estimate the total exported flux. Three aliquots were then weighed to estimate total carbon, POC as well as particulate trace metals exported during the experiment: Fe and Cu.

Total carbon was measured with a CHN elemental analyzer (2400 Series II CHNS/O Elemental Analyzer, Perkin Elmer®) on weighted subsamples. POC was measured similarly, after removing inorganic carbon by acidification with 2 N HCl.

Particulate Fe and Cu concentrations were measured by ICP-OES (Inductively Coupled Plasma Optical Emission Spectrometry; Perkin-Elmer® Optima-8000) on acid-digested samples. Digestions were performed in Teflon® vials by adding Suprapur grade acids to weighed subsamples in two steps: (1) 1 mL of 65% nitric acid (HNO_3) followed by a mixture of (2) 500 μL of 65% HNO_3 and 500 μL of 40% hydrofluoric acid. After each step, samples were heated at 150°C for 5 h. Several aliquots of blanks and certified reference material (GBW, NRCC) were digested and analyzed under the same conditions. Blanks (reagent alone and reagent + blank filter) were below the detection limit (DL). The percentage recovery obtained with the certified reference material indicated accurate digestion and quantitative analysis for all elements (Fe: 94 ± 4%, Cu: 97 ± 3%).

2.2.6 Statistical analyses

To estimate whether the addition of different hydrothermal fluid volumes had an effect on the measured parameters as a function of time, multiple linear regressions with interaction were performed following James et al. (2013). These regressions were modeled to follow the formula $y = ax_1 + bx_2 + c$, with y, the parameter of interest; x_1, the mixing ratio (in %); x_2, the sampling time and c, the intercept. In order to compare the growth and decline phases of the control to the kinetics observed in the fluid-enriched treatments, regressions were performed independently at the start (12 h, 24 h, 48 h) and at the end (96 h, 144 h, 216 h) of the experiment *via* the *lm* function in R software. In case of significant interaction (*p-value (p)* < 0.05), a pairwise *post-hoc* comparison test was performed to determine the percentage(s) of enrichment having an effect on the considered parameter using the *emmeans* package (Lenth et al., 2019).

3 Results

Irradiance, temperature and pH on the total scale during the experiment are shown in Figure S1. Briefly, the different L:D cycles (Light : Dark) were stable for all minicosms. The targeted experimental temperature (25.7°C) was achieved in each minicosm, although a lower temperature (25.2°C) was recorded in

10.3389/fmars.2023.1082077

the +9.1% fluid treatment. However, this value was within the range of *in-situ* surface temperatures and likely did not significantly impact the results presented. Since the pH of the fluid end-member was very low (~6.5), decreases in pH proportional to the addition of fluid were observed. These pH values gradually returned to the values observed *in-situ* in surface waters, due to CO_2 outgassing during the experiment. Dilution curves performed on pH, nutrients and DFe data are shown in Figure S2 and attest the accuracy and quality of the mixing performed.

3.1 Dissolved iron

DFe concentration ([DFe]) in the fluid end-member was 15-fold higher than in the surface end-member. [DFe] followed quite similar dynamics in all fluid-enriched treatments (Figure 2). They increased until day 1, peaking at 3.2-19.5 nmol L^{-1}, before gradually decreasing until the end of the experiment.

In the following section, the results will be discussed according to two selected periods of the experiment: period 1 (P1) from the start of the experiment to day 2 and period 2 (P2) from day 2 to the end of the experiment.

3.2 Stocks and fluxes during the experiment

3.2.1 Biological stocks

3.2.1.1 Cyanobacteria

Prochlorococcus abundance increased in all minicosms during P1, independent of fluid treatment ($p > 0.05$; Figure S3A), although the maximum abundances reached were 1.1 to 2-fold higher in the fluid-enriched treatments relative to control (Table 2), except for the +3.6 and +10.9% fluid treatments. *Prochlorococcus* populations then gradually decreased until the end of P2, independently of the treatment ($p > 0.05$; Figure S3A). In contrast, *Synechococcus* populations showed significant differences between the fluid-enriched treatments and the control ($p < 0.05$; Figure S3B). Control populations increased until day 1 only, before decreasing. Population in the +7.3% fluid treatment followed the same kinetics as in the control, although the maximum abundance was two-fold higher (Table 2). Comparatively, *Synechococcus* grew in all other fluid-enriched treatments until day 2, reaching up to 8-fold higher maximum abundance as compared to the control. *Synechococcus* populations decreased in most minicosms during P2, even reaching a near-zero abundance in some treatments ($p > 0.05$; Figure S3B). Modest increases in abundance were observed for three of the seven fluid-enriched treatments between days 6 and 8. Only the +1.8% fluid treatment reached its maximum abundance in P2 (x3.7 relative to the control; Table 2).

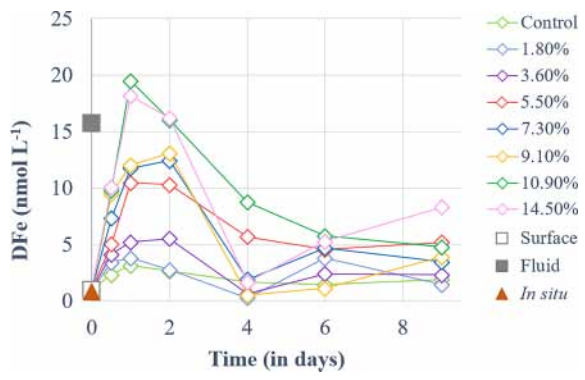

FIGURE 2
Temporal dynamics of dissolved iron (DFe) concentrations for a gradient of fluid addition (in % of total minicosm volume). DFe concentrations measured in the surface and fluid end-members are represented by an empty and a solid gray square, respectively. The red triangle represents the concentration measured *in-situ* above the sampled hydrothermal source at 5 m during the CTD casts of TONGA cruise.

3.2.1.2 Non-cyanobacterial phytoplankton

Haptophyceae biomass (B_{hapto}) in the control increased throughout P1 (Figure 3A) before decreasing during P2. In comparison ($p < 0.01$), no increase in biomass was observed in the fluid-enriched treatments during P1, as B_{hapto} decreased (reaching ~0.004 µg L^{-1}) relative to the initial biomass (0.01 µg L^{-1}). During P2, B_{hapto} continued to increase until day 4, peaking at 0.035 µg L^{-1}, before gradually decreasing (Figure 3A). Stagnant in P1, B_{hapto} in fluid-enriched treatments increased throughout P2, reaching values twice the one in the control (up to 0.1 µg L^{-1}, $p < 0.01$). Diatom biomass (B_{dia}) remained stable in the control (~0.0031 µg L^{-1}) within the first 24 h relative to the initial biomass (0.0025 µg L^{-1}). It then doubled at the end of P1 (Figure 3B) and remained stable throughout P2 (~0.0025 µg L^{-1}). B_{dia} in the fluid-enriched treatments remained stable during P1 at much lower values than those reached in the control ($p < 0.002$). It then increased from the start of P2 until day 6. B_{dia} then stabilized in most fluid-enriched treatments, except for the +5.5, +7.3 and +10.9% fluid treatments in which a significant increase was observed at the end of P2 (up to 0.043 µg L^{-1}; $p < 0.006$ relative to the control). Dinoflagellate biomass (B_{dino}) in the control increased throughout P1, peaking at 0.046 µg L^{-1} before decreasing until the end of P2 (Figure 3C). The opposite was observed in the fluid-enriched treatments, displaying a decreasing trend ($p < 0.001$) during P1 (~0.001 µg L^{-1}), which continued until day 4. It stabilized between 4 and 6 days before increasing significantly in the fluid-enriched minicosms until the end of P2 ($p < 0.05$ relative to control).

3.2.2 Biological fluxes

Cumulative NCP increased during P1 similarly in all treatments ($p > 0.08$, Figure 4A). At the start of P2, a slight shift occurred: while control NCP continued to increase, NCP in fluid-enriched treatments stabilized until day 6 (except for the +14.5% fluid treatment; Figure 4A). Control NCP stabilized after 4 days, peaking at 19.8 µmol C L^{-1}, before decreasing. In comparison, cumulative NCP in fluid-enriched treatments finally increased significantly at the end of P2, to higher levels than in the control (~30.6 µmol C L^{-1}, $p < 0.04$). A strong positive correlation was observed between the maximum cumulative NCP reached for each treatment and the percentage of fluid enrichment ($R^2 = 0.72$, $p < 0.05$; Figure 4B).

10.3389/fmars.2023.1082077

TABLE 2 Ratio of maximum relative changes in biomass of cyanobacteria populations in hydrothermal fluid-enriched treatments relative to the control.

Treatment	*Prochlorococcus*	*Synechococcus*
1.8%	1.1 (day 2)	3.7 (day 8)
3.6%	0.7 (day 2)	4.3 (day 2)
5.5%	1.4 (day 2)	4.6 (day 2)
7.3%	1.6 (day 2)	2.1 (day 1)
9.1%	1.5 (day 2)	7.5 (day 2)
10.9%	0.9 (day 2)	3.4 (day 2)
14.5%	2.0 (day 2)	4.3 (day 3)

The sampling time at which these maximum relative changes were observed is indicated in parentheses. The abundance of cyanobacteria (*Prochlorococcus* and *Synechococcus*) was measured by flow cytometry.

Cumulative N_2 fixation (Figure 4C) also increased in all minicosms during P1. It stabilized in the control at the end of P1 while it continued to increase, although less sharply, in the fluid-enriched treatments. Cumulative N_2 fixation in the control remained stable during P2, peaking at 15 nmol N L^{-1} (Figure 4C). In comparison, N_2 fixation continued to increase throughout P2 in the fluid-enriched treatments, reaching values 2.5-fold higher than the control. No significant correlation was found between the maximum cumulative N_2 fixation reached for each treatment and the percentage of fluid added (R^2 = 0.019, p = 0.96).

3.2.3 Dissolved organic compounds

3.2.3.1 Thiols

Two types of thiol compounds were identified during the experiment: TA and GSH compounds. TA concentrations ([TA]) remained stable in the control during both P1 and P2 (~92.8 nmol L^{-1}; Figure S4A). In contrast, [TA] increased at the start of P1 in all fluid-enriched treatments, reaching a maximum concentration 2.5- to 9.2-fold higher than in the control (p < 0.04; Table 3). However, no correlation between the percentage of fluid enrichment and [TA] increase was observed (R^2 = 0.41, p = 0.31). [TA] then decreased rapidly until the end of P2, reaching near-control levels. GSH concentrations ([GSH]) were null in all minicosms at the start of P1 (Figure S4B). They started to increase at P2, except for the +1.8% and the +9.1% fluid treatments, reaching concentrations 1.1 to 1.9-fold higher than in the control (Table 3).

3.2.3.2 Fluorescent dissolved organic matter

Three FDOM fluorophores were identified by the PARAFAC model: two protein-like fluorophores, i.e., tryptophan-like (TP; peaks T) and tyrosine-like (TY; peaks B), and one humic-like fluorophore (HS; peaks 1+C). These are the most prevalent FDOM fluorophores in the aquatic environment (Coble, 2007; Aiken, 2014). Below, fluorophore concentrations refer to their fluorescence intensities in QSU.

TP concentrations ([TP]) increased in all fluid-enriched treatments during P1 (Figure S5A), whereas [TP] remained stable in the control (p < 0.01). Only the +3.6% fluid treatment reached its maximum concentration during P1 which was lower than in the control (Table 3). [TP] slightly increased throughout P2 (Figure S5A), mainly in the fluid-enriched treatments, reaching maximum concentrations 1.3 to 3.3-fold higher than in the control (Table 3). A drastic increase of TY concentrations ([TY]) was observed in all minicosms during P1. Only [TY] in the control decreased after 24 h (Figure S5B). HS concentrations ([HS]) increased during the first 24 h in all minicosms before stabilizing until the end of P1 (Figure S5C, p > 0.05). [TY] and [HS] followed the same dynamics as [TP] during P2 (p < 0.03), reaching maximum concentrations 1.1 to 1.4 higher in the most enriched minicosms as compared to the control.

3.3 Trace metal and POC concentrations in exported material collected in particle traps throughout the experiment

The exported material from the control, +3.6% and +10.9% fluid treatments showed similar Fe concentrations ([Fe]; ~3.67 mg g^{-1}; Figure 5A). [Fe] from other fluid-enriched treatments doubled relative to the control. The highest [Fe] (x4 relative to the control)

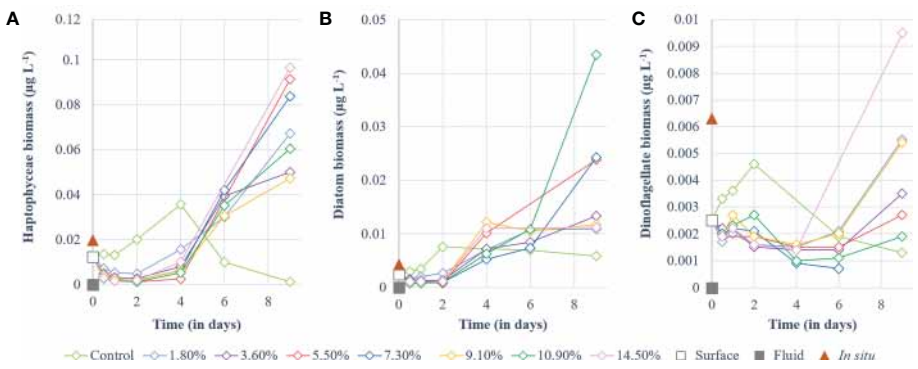

FIGURE 3
Temporal dynamics of non-cyanobacterial phytoplankton biomass (µg L^{-1}) for a gradient of fluid addition (in % of total minicosm volume). **(A)** haptophyceae (i.e., 19'-hexanoyloxyfucoxanthin), **(B)** diatoms (i.e., fucoxanthin) and **(C)** dinoflagellates (i.e., peridinin). Values measured for each pigment in the surface and fluid end-members are represented by an empty and a solid gray square, respectively. The red triangle represents the value measured *in-situ* above the sampled hydrothermal source at 5 m during the CTD casts of TONGA cruise.

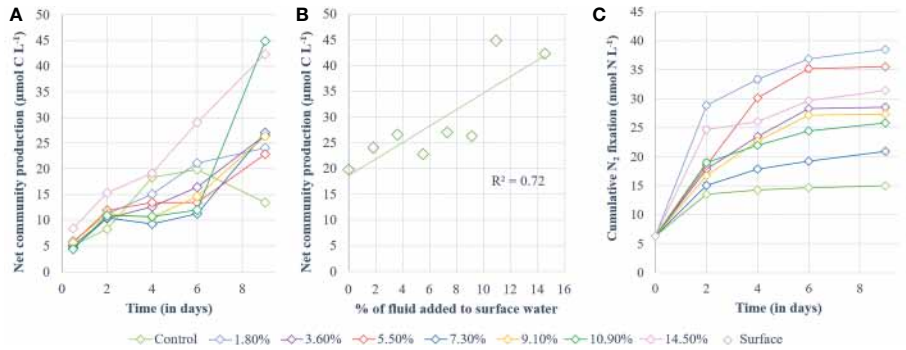

FIGURE 4
Processes studied during the experiment. **(A)** cumulative ^{13}C-net community production and **(B)** highest values of cumulative ^{13}C-net community production obtained for each minicosm (i.e., day 6 for the control and day 9 for the fluid-enriched treatments) correlated with the percentage of hydrothermal fluid added. Net community production is shown in µmol C L^{-1} and was determined according to the ^{13}C-labeling method described by de Kluijver et al. (2010). **(C)** Cumulative dinitrogen fixation (nmol N L^{-1}).

was observed in the most fluid-enriched treatment. Nevertheless, no significant correlation was found between the exported [Fe] and the percentage of fluid added (R^2 = 0.24, p = 0.57). High concentration of Cu ([Cu]) were exported in the most fluid-enriched treatments relative to the control (x2.4; Figure 5B). However, low [Cu] was exported in the +5.5% and +9.1% fluid treatments relative to the large volume of fluid added. Nevertheless, a positive relationship between the [Cu] exported and the percentage of fluid added was observed (R^2 = 0.6, p = 0.03). POC concentrations ([POC]) exported in the fluid-enriched treatments were higher than the control (x1.4), except for the +3.6% fluid treatment that exported lower [POC] (Figure 5C). The highest [POC] (x2 relative to the control) were exported in the least fluid-enriched treatment. No correlation between the [POC] and the percentage of fluid added was found (R^2 = 0.27, p = 0.52).

4 Discussion

Our primary concern was whether the dynamics observed for the major phytoplankton groups and thiols were a consequence of the biological response to the addition of hydrothermal fluids or a dilution effect following the mixing of the two end-members. Theoretical dilution lines were thus calculated for each treatment and compared to the measured values of the parameters at 12 h (Figure S6). For the cyanobacteria biomass, the measured values were always higher (~0.08 µg L^{-1}) compared to theoretical values (~0.05 µg L^{-1}), indicating that cyanobacteria developed rapidly after mixing. In comparison, measured values of B_{hapto} (~0.004 µg L^{-1}) and B_{diato} (~0.001 µg L^{-1}) were lower than theoretical values (~0.01 µg L^{-1} and ~0.003 µg L^{-1}, respectively) in the fluid-enriched treatments, showing a decline of both after mixing. The opposite was observed in the control (i.e., higher measured than theoretical values). Regarding thiols, while measured and theoretical [TA] of the control matched perfectly, [TA] measured in fluid-enriched treatments were up to 8 times higher than theoretical [TA]. This evidence shows that the dynamics observed during the first 12 h after mixing were rather a biological response to hydrothermal fluid enrichment than a simple dilution effect.

4.1 Primary effect of fluids

In the control minicosm, a small increase of biomass associated with picocyanobacteria, haptophyceae, diatoms and dinoflagellates was observed during P1. This increase lasted for only two days,

TABLE 3 Ratio of maximum relative changes in the concentrations of thiol compounds and fluorescent dissolved organic matter (FDOM) fluorophores in hydrothermal fluid-enriched treatments relative to control.

Treatment	Thiols		FDOM fluorophores		
	TA-like	GSH-like	Tryptophan-like	Tyrosine-like	Humic-like
1.8%	3.7 (day 0.5)	0.68 (day 9)	1.3 (day 9)	1.3 (day 9)	1.1 (day 9)
3.6%	3.8 (day 0.5)	1.7 (day 4)	0.8 (day 2)	1.2 (day 6)	1.2 (day 9)
5.5%	2.9 (day 0.5)	1.9 (day 4)	1.6 (day 9)	1 (day 6)	1.4 (day 9)
7.3%	2.5 (day 0.5)	1.2 (day 4)	2.3 (day 9)	1.2 (day 9)	1.4 (day 9)
9.1%	2.5 (day 0.5)	1 (day 9)	1.7 (day 9)	1.2 (day 4)	1 (day 9)
10.9%	2.6 (day 0.5)	1.3 (day 9)	3.3 (day 9)	1.2 (day 4)	1.2 (day 9)
14.5%	9.2 (day 0.5)	1.1 (day 9)	1.5 (day 6)	0.9 (day 9)	1.2 (day 9)

The sampling time at which these maximum relative changes were observed is indicated in parentheses. TA refers to thioacetamide-like thiol compounds while GSH refers to glutathione-like thiol compounds. FDOM is composed of two protein-like (tryptophan- and tyrosine-like) and one humic-like fluorophores. Concentrations of the three fluorophores refer to their fluorescence intensities in QSU.

10.3389/fmars.2023.1082077

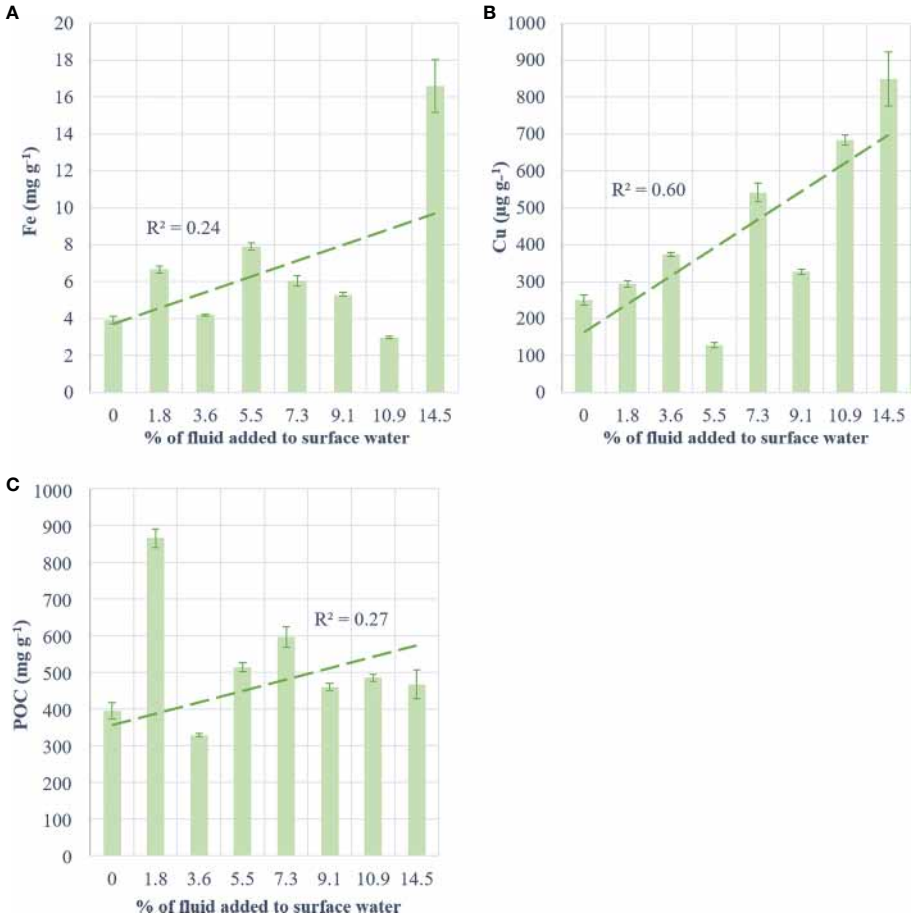

FIGURE 5
Concentration of metals and carbon per g of collected matter in traps at the end of the experiment for **(A)** iron (mg g^{-1}), **(B)** copper (µg g^{-1}) and **(C)** particulate organic carbon (mg g^{-1}) as a function of treatment (+0 to +14.5% hydrothermal fluid added). The green dotted line represents the regression line and its coefficient (R^2).

probably due to nutrient limitation, especially in nitrate (< 0.1 µmol L^{-1}, Figure S7; Bonnet et al., in rev.). The biomass associated with those groups then decreased rapidly until the end of the experiment. Nevertheless, this brief development at the start of the experiment resulted in fairly significant cumulative NCP and POC export into the traps. In contrast, N_2 fixation rates remained stable during this period in the control, and throughout the experiment.

Large differences were observed between the control and fluid-enriched treatments regarding community composition, plankton abundance and biological fluxes. Indeed, at the start of P1, only picocyanobacteria (mainly *Synechococcus)* developed after the mixing and at much higher abundances than in the control. Yet, the fluids provided a small amount of macronutrients that could have supported the growth of phytoplankton (+0.04-0.28 and +0.003-0.023 µmol L^{-1} of $NO_3^-$and PO_4^{3-} added by fluids, respectively, relative to the control; Bonnet et al., in rev.). Furthermore, active diazotrophs also likely provided new N sources to the system. Compared to the control, the large non-cyanobacterial species did not develop during P1 and dinoflagellate mortality (i.e., decreased abundance) was even observed. One possible hypothesis is that the observed patterns were the result of an initial toxicity of some elements supplied by the fluids. Such an effect would have decreased after 4 days of experiment, as species whose growth was stagnant finally started to grow. This implies that the studied waters had likely been detoxified, consistent with the dynamics of thiols at P1, as these compounds have been reported to selectively complex certain toxic trace metals (Grill et al., 1989; Ahner and Morel, 1995; Zenk, 1996). This mechanism will be explored in the following section.

4.2 Detoxification of the environment and candidate toxic elements

Environmental detoxification may occur through the excretion of metal-binding ligands by communities (e.g., Leal et al., 1999; Morel and Price, 2003; Dupont and Ahner, 2005; Hoffmann et al., 2012). Two types of organic ligands capable of detoxifying the environment were measured during the experiment: FDOM, protein- and humic-like fluorophores, and thiols, a pool of non-fluorescent matter (Chen et al., 2013). In this section, an in-depth exploration of thiol implication in environmental detoxification will be conducted. FDOM fluorophores will be discussed in accordance with their role as strong Cu ligands (Wong et al., 2019).

Thiol production by phytoplankton is triggered by the presence of various trace metals such as Cd, Cu, Hg, Pb and Zn (Grill et al., 1989; Ahner and Morel, 1995; Zenk, 1996). These metals, essential (Cu, Zn) or not (Cd, Hg, Pb), can cause numerous deleterious effects on communities at various concentrations (e.g., Sunda and Huntsman, 1998; Echeveste et al., 2012; Le Faucheur et al., 2014). During our experiment, communities immediately responded to fluid addition through striking thiol production (i.e., up to +823% [TA] relative to control produced during the 12 h after the mixing). Two types of thiol compounds were detected: TA and GSH. TA is actively exuded by phytoplankton (Leal et al., 1999) and precipitates trace metals, rendering them non-bioavailable to communities (Gharabaghi et al., 2012). GSH is the most common thiol ligand in surface waters (Le Gall and Van Den Berg, 1998; Leal et al., 1999; Tang et al., 2000) and is a precursor of phytochelatins (PC; Grill et al., 1989), a polypeptide that forms complexes with trace metals ultimately transported and degraded in the vacuole and/or chloroplasts (Cobbett, 2000; Worms et al., 2006). Thus, the decrease in [GSH] to near-zero levels reflects a high PC production (Romano et al., 2017). Previous studies reported that GSH levels in the presence of high metal concentrations could reach undetectable levels within a few hours (2-4 h; Scheller et al., 1987; Coppellotti, 1989; De Vos et al., 1992; Rijstenbil et al., 1994; Satoh et al., 1999), in agreement with the levels observed in minicosms 12 h after the mixing (< DL). After the probable environmental detoxification, [GSH] accumulated in minicosms. This result was expected as GSH also plays a homeostasis and environmental sensing role in phytoplankton (May et al., 1998; Noctor et al., 1998). Thus, these two thiol compounds had a key role in mitigating the deleterious effects of toxic trace metals added to the environment by fluids (Figure 6). The possible trace metals released by hydrothermal fluids will be explored in this section in accordance with their ability to trigger thiol production (i.e., Cd ≥ Cu > Pb > Hg; Grill et al., 1989; Ahner and Morel, 1995).

4.2.1 Cadmium

Cd has been reported as the most effective trigger of thiol production in most phytoplankton species (Ahner and Morel, 1995; Dupont and Ahner, 2005; Romano et al., 2017; Permana and Akbarsyah, 2021). Consistently, elevated concentrations of particulate Cd were measured in the fluid end-member relative to the surface end-member (x11.5; Table S2) suggesting that fluid addition supplied high Cd levels. This raises the possibility that Cd played a role in the preliminary toxicity induced by shallow hydrothermal fluid addition.

4.2.2 Copper

Cu has been reported to trigger significant phytoplankton production of thiols, both TA and GSH, their presence allowing for rapid and efficient detoxification of the environment (De Vos et al., 1992; Leal et al., 1999; Brown and Gordon, 2001; Dupont and Ahner, 2005). Although total dissolved Cu (DCu) concentrations were similar in fluid and surface end-members (~250 pmol L^{-1}), DCu toxicity depends solely on the concentration of the free Cu^{2+} form (not measured during TONGA), the only toxic form of DCu and also the most bioavailable (Brand et al., 1986; Ahner et al., 1994; Sunda, 1994; Ahner et al., 1998). Interestingly, shallow hydrothermal sources have been reported to release high concentrations of labile material, including Cu^{2+} (Valsami-Jones et al., 2005; Hawkes et al., 2014), suggesting that a significant portion of the DCu measured in the fluid end-member may be in the ionic form. Thus, the low concentration of DCu present in the fluid could still be extremely toxic to communities, as Cu^{2+} concentrations as low as 2.3 pmol L^{-1} have been reported to be toxic to some species (Leal et al., 1999; Mann et al., 2002). In contrast, an 82-fold enrichment of particulate Cu (pCu) in the fluid end-member relative to the surface end-member was measured (Table S2). A relationship between the percentage of fluid addition and the concentration of exported pCu (Figure 5) was also found. This pCu was probably a mixture between fluid-added hydrothermal particles and Cu-TA compounds (i.e., complexed thiols). However, based on pCu concentrations added by fluid and surface end-members (see Text S5 for further details), it can be stated that not all of the added pCu was recovered in the material exported in fluid-enriched treatments (~28-72% recovered depending on the fluid addition), in contrast to the control (101% pCu recovered). This could be explained by a possible redissolution of hydrothermal particles at the start of the experiment (favored by the low pH; Figure S1; Ain Zainuddin et al., 2019) or by the presence/formation of fine particles that may be slow to settle. This is likely as most hydrothermal particles have been reported to have a small diameter (< 2 µm; Walker and Baker, 1988) and Lou et al. (2020) demonstrated that particles smaller than 20 µm were

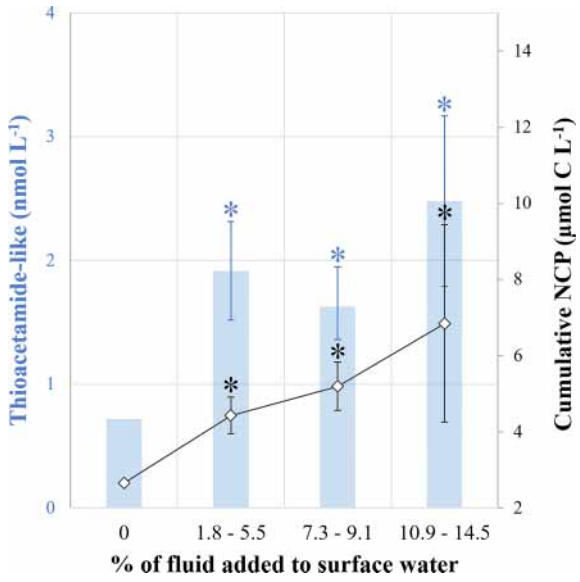

FIGURE 6
Summary diagram. (1) in blue, the ratio of thioacetamide-like compound concentrations measured 12 h after the mixing versus at the end of the experiment (D0.5:D9) and, (2) in black, the ratio of cumulative ^{13}C-net community production rates measured at the end versus at the start of experiment (D9:D0.5). Treatments were grouped: no addition (0, control), low (+1.8-5.5%), medium (+7.3-9.1%) and high (+10.9-14.5%) fluid addition. Asterisks represent the significance of each group relative to control (*unpaired Student test*, $p < 0.01$).

involved in the long-distance transport of the plume (and thus have a lower sedimentation rate). Furthermore, a high FDOM production was observed in the fluid-enriched treatments with significant increases in the concentrations of protein- and humic-like fluorophores during the experiment (Table 3). Besides thiols compounds, protein- and humic-like fluorophores have been clearly identified as organic ligands that present binding affinities with trace metals, particularly Cu^{2+} (Mounier et al., 2011; Chen et al., 2013). A recent study also showed a strong correlation between FDOM production, Cu^{2+} concentrations and L_1-class ligands in marine waters (Wong et al., 2019). All these observations suggest a release of protein-like FDOM by phytoplankton in response to Cu toxicity (Corbett, 2007; Wong et al., 2019). Thus, Cu may play an important role in the toxicity induced by fluid addition at the start of the experiment.

4.2.3 Lead

Pb is a known trigger for thiol production by phytoplankton, although less effective (Ahner and Morel, 1995). This element may have had a toxic effect on communities subjected to fluid enrichment at the start of the experiment, as particulate Pb was 91 times enriched in the fluid end-member relative to the surface end-member (Table S2).

4.2.4 Mercury

Hg has been reported as being one of the less effective triggers of thiol production by phytoplankton in response to toxic environments (Satoh et al., 2002; Wu and Wang, 2012). Despite such a fact, total Hg (THg) concentrations in the fluid end-member were 10 times higher than in the surface end-member (Table S2, Desgranges, pers. comm., 2022). THg was present primarily as elemental Hg (i.e., in gaseous form; Desgranges, pers. comm., 2022) that can (1) degas to the atmosphere and/or (2) be oxidized to Hg^{2+} reported to be extremely toxic to phytoplankton (Wu and Wang, 2011). Even if it is impossible to conclude which Hg form predominates in fluid-enriched treatments, high concentrations of Hg^{2+} could be toxic, or even lethal, to communities.

Other thiol-complexed trace metals, such as Zn or nickel, were not exported in significant amounts in traps relative to the control. It is therefore unlikely that these elements played a significant role in the biological dynamics observed during P1. Thus, the high production of thiols in response to the hydrothermal fluid addition is coherent and could be triggered by the presence of a cocktail of several toxic elements such as Cu, Hg, Pb and possibly Cd.

4.3 The most probable producers of thiol ligands

The question of which players produce thiols capable of detoxifying the environment is relevant. In the present experiment, picocyanobacteria could be the potential thiol producers (Moffett et al., 1990; Moffett and Brand, 1996; Croot et al., 2000). In fact, the first organisms to grow were picocyanobacteria such as *Synechococcus* and *Prochlorococcus* to a lesser extent, consistent with the striking increase of thiols that occurred 12 h after the mixing (Table 3). In line with these observations, *Prochlorococcus* has been reported to be more sensitive to trace metal addition than *Synechococcus* (Mann et al., 2002). However, *Synechococcus* has previously been reported as one of the most sensitive species to trace metal addition due to its large surface-to-volume ratio (Quigg et al., 2006). This was not observed in this experiment, as in several other studies, where *Synechococcus* was the most resistant species to trace metal addition while eukaryotic species were the most sensitive (Joux-Arab et al., 2000; Stauber and Davies, 2000; Le Jeune et al., 2006; Levy et al., 2007). Numerous studies have demonstrated the existence of *Synechococcus* ecotypes adapted to toxic trace metal concentrations, either genetically or physiologically (Huckle et al., 1993; Mann et al., 2002; Palenik et al., 2006; Stuart et al., 2009; Stuart et al., 2013). These ecotypes are primarily from environments where trace metal concentrations may be chronically high, such as coastal waters or near hydrothermal vents, and are adapted to a fast-changing environment (Mann et al., 2002; Stuart et al., 2009). They may also be related to their previous exposure to trace metals (Levy et al., 2007). Low abundance of cyanobacteria was measured in the fluid end-member (0.0035 $\mu g\ L^{-1}$). It is therefore possible that the thiol-producing *Synechococcus* adapted ecotypes found in fluid-enriched treatments originated from the environment near the shallow hydrothermal source and allowed for environmental detoxification. Molecular analyses would be necessary to confirm such a hypothesis. For all these reasons, it is very likely that *Synechococcus*, known to produce strong binding ligands, including thiols (Moffett et al., 1990; Moffett and Brand, 1996; Croot et al., 2000), was the major producer of these ligands that were needed to inhibit toxicity of ionic trace metal, allowing other species to grow. Moreover, Brand et al. (1986) demonstrated that *Synechococcus* growth rates subjected to high concentrations of Cu or Cd were inhibited in the absence of strong chelators.

Based on our experimental data, the largest non-cyanobacterial species (haptophyceae, diatoms and dinoflagellates) were probably not the major thiol producers, especially since eukaryotes have been reported to have more affinity for thiols-Cu complexes, in contrast to prokaryotes (Walsh et al., 2015) and to produce weaker ligands (Croot et al., 2000). Indeed, diatoms and haptophyceae only developed 2 and 4 days after the mixing, respectively, not coinciding with the thiol peaks measured 12 h after mixing. However, it is interesting to note that diatoms – known to be more tolerant to the addition of certain trace metals, such as Cu (Croot et al., 2000) – were the first to develop after environmental detoxification. Dinoflagellate mortality (i.e., decrease in biomass) was observed from the start of the experiment, rendering these species poor candidates for strong ligand production. This result is not surprising as dinoflagellates are known to be very sensitive to Cu, even at low concentrations, and to other trace metals (Anderson and Morel, 1978; Brand et al., 1986; Taylor, 1987; Lage et al., 2001). Encystment strategies have been developed by dinoflagellates to protect themselves from a harmful environment (Anderson and Morel, 1978; Pinto et al., 2003), allowing the persistence of plasma membrane and chlorophyll integrity (Lage et al., 2001). Recovery from trace metal exposure has been observed for numerous dinoflagellates species within 24 to 96 h after exposure (Lage et al., 1994; Okamoto et al., 1999). This excystation process may

explain the delayed growth of dinoflagellates (6 days after the mixing) relative to other species.

Abiotic factors such as pH and temperature and biotic factors such as uptake pathways and internal detoxification processes can influence trace metal tolerance. When mixing the two end-members, addition of one (or a cocktail of) trace metal(s) and H_2S-rich, low-pH and oxygen-poor fluid (Tilliette et al., 2022) temporarily altered the surface water chemistry and may have exacerbated the toxic effect of fluid addition. Nevertheless, due to the significant production of thiols by picocyanobacteria, especially by resistant *Synechococcus* ecotypes, potential toxic elements supplied by hydrothermal fluids have been modified into less harmful forms. This environmental detoxification allowed the larger species to grow and a late positive effect proportional to the fluid addition could be observed at the end of the experiment (see the following section).

4.4 Fertilizing effect of fluid addition and comparison with *in situ* data

As discussed above, the addition of hydrothermal fluids to surface waters first inhibited biological activity until the fluid chemistry was modified by the production of thiols making the mixed water less harmful or even fertilizing (Figure 6). Indeed, growth of non-cyanobacterial species was observed 4 days after the mixing, resulting in enhanced cumulative NCP rates (up to x3.3 relative to the control) at the end of the experiment. Moreover, an increasing fertilizing effect depending on the addition of hydrothermal fluid was observed, as the maximum cumulative NCP values were proportional to the percentage of fluid added (Figure 4B). This positive effect was also observed for N_2 fixation, which was up to 2.5-fold higher in fluid-enriched treatments relative to the control. Consequently, an increase of POC export was measured in the fluid-enriched treatments (x1.4 on average and up to x2.2 relative to the control). Such a positive effect on NCP and N_2 fixation is likely due to the introduction of high concentrations of fertilizing elements, such as Fe, along with rather low concentrations of macronutrients, so the system was likely still nitrate-limited. During the TONGA cruise (Guieu and Bonnet, 2019), the same stocks and fluxes studied in the minicosms were measured *in-situ* along a 6100-km transect through the Tonga volcanic arc. Cruise results show that N_2 fixation rates were the highest above hydrothermal sources and primarily supported by large (> 10 µm) species such as *Trichodesmium* (Bonnet et al., in rev.). In contrast, *in-situ* primary production was high a few kilometers from the source, but lower just above it (Bonnet, *unpublished*), likely reflecting the toxic effect of fluids evidenced during our experiment.

Fe is an essential element for phytoplankton growth and metabolism (Behrenfeld and Milligan, 2013). It is a known fertilizing element for all phytoplankton species, having a direct influence on photosynthesis (Sunda and Huntsman, 1995) and thus an important role in carbon export and sequestration in the ocean interior (Martin, 1990; Pollard et al., 2007). Fe is also often a limiting element for diazotrophs, as in addition to photosynthesis, the N_2 fixation process also requires high Fe amounts (Raven, 1988). During the experiment, hydrothermal fluids supplied high Fe concentrations, both in particulate and dissolved forms (Figure 4). Indeed, a 772- and 16-fold enrichment of particulate (Table S2) and dissolved Fe, respectively, could be observed in the fluid end-member relative to the surface end-member. These high DFe concentrations introduced by the fluid end-member ([DFe] = 15.8 nmol L^{-1}) were likely responsible for the high N_2 fixation and NCP rates measured in the fluid-enriched treatments. This was confirmed (see Text S6) by the higher Fe uptake rates of picocyanobacteria (mainly *Synechococcus* and bacteria), that consumed up to 16% of the total minicosm DFe stock over the course of the experiment, relative to non-cyanobacterial species, that consumed up to 8% of the total stock, in agreement with the uptake rates measured by Lory et al. (2022) during the TONGA cruise (~4-11 pmol Fe L^{-1} d^{-1}). Interestingly, consistent with these uptake rates, the DFe dynamics observed during the experiment were primarily driven by precipitation. This process can easily be explained by the presence of high H_2S concentrations in the fluid (Tilliette et al., 2022) and the gradual increase in pH, which was significantly decreased at the start of the experiment through the low pH fluid addition (pH of 6.5; Figure S1). Estimated precipitation rates in fluid-enriched treatments (66 ± 7%) were similar to those estimated *in-situ* above the shallow hydrothermal source (62-86%; Tilliette et al., 2022). As for Cu, only a small proportion of the particulate Fe was recovered in traps (< 10%), probably due to the small particle size that did not allow them to be exported.

The growth of the large non-cyanobacterial species occurred at days 2-4, when phosphate and nitrate concentrations were nearly depleted (Bonnet et al., in rev.; Figure S4). Nitrogen was made available to non-diazotrophic phytoplankton through N_2 fixation and the use of rather abundant DOP (~0.2 µmol L^{-1} after 4 days, *data not shown*) as an alternative P-source may have allowed their growth. Indeed, microbial utilization of DOP through alkaline phosphatase activity can be Fe-limited (Browning et al., 2017) and the alleviation of Fe stress leads to DOP loss (likely as a consequence of enhance uptake) under low phosphate availability at the global scale (Fernández-Juárez et al., 2019; Liang et al., 2022). Thus, the introduction of high concentrations of DFe by the fluid end-member mitigated the Fe limitation of surface end-member waters. This DFe fertilization by fluids is of great importance as diazotrophs can exploit these high concentrations to build biomass, as long as phosphate concentrations are sufficient or if these organisms also use DOP (Dyhrman et al., 2006; Dyhrman and Haley, 2006). The fluid addition also allowed an important enrichment in Al (x27.5 of particulate Al relative to control; Table S2). Interestingly, Al has been reported to promote Fe uptake (Shaked et al., 2005; Mujika et al., 2011; Ruipérez et al., 2012), DOP utilization and N_2 fixation (Liu et al., 2018) and may explain, in addition to DFe availability, the fertilizing effects observed on phytoplankton communities over half of the experiment. Subsequent nitrogen provision by these organisms in this N-poor environment likely allowed the development of larger non-diazotroph species (i.e., haptophyceae, diatoms and dinoflagellates), which in turn likely also explains the observed significant impact on primary production (Berthelot et al., 2016). Hydrothermal fluid-induced DFe fertilization, which resulted in higher primary production rates and POC export, indicated that such fertilization has a positive impact on the biological carbon pump, in line with *in-situ* results obtained during the TONGA cruise (Bonnet et al., in rev.). It should be noted that the experiment had to be stopped for logistic reasons, during the exponential phase of

10.3389/fmars.2023.1082077

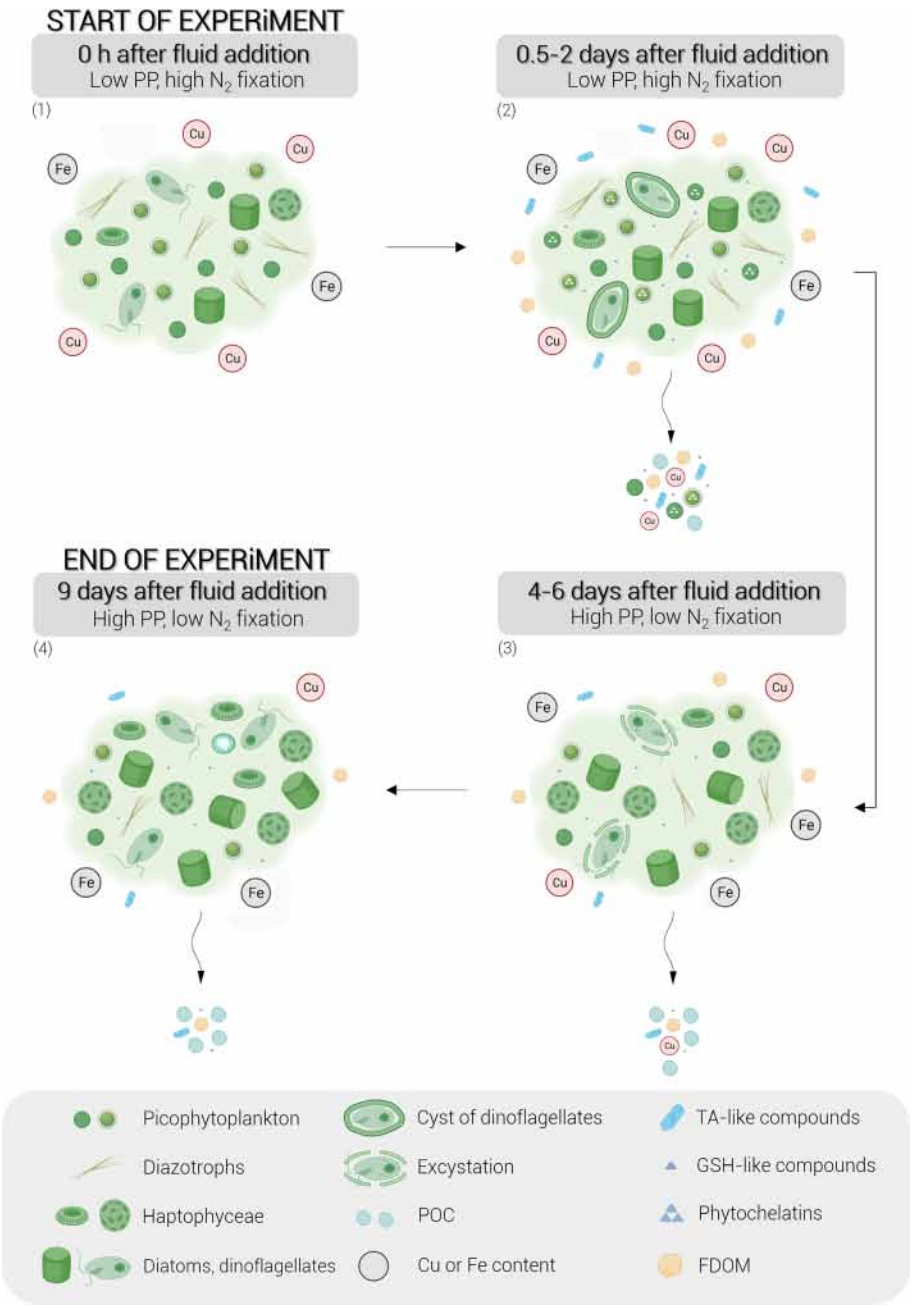

FIGURE 7
Conceptual diagram of the stepwise biological responses of natural phytoplankton communities to hydrothermal fluid addition during the nine-day experiment. Briefly, the following points can be observed: (1) the dominance of picocyanobacteria and diazotrophs at the start of the experiment due to the toxicity of the metals supplied by the hydrothermal fluid, (2) the production of organic ligands by *Synechococcus*, in particular thiols and FDOM, within 0.5 to 2 days after the fluid addition, (3) the development of eukaryotic phytoplankton following environmental detoxification, leading to high primary production and (4) the exponential growth of these eukaryotes until the end of the experiment. The schematic legend is represented in a grey frame. Cu, copper; Fe, iron; TA-like compounds, thioacetamide-like compounds; GSH-like compounds, glutathione-like compounds; FDOM, fluorescent dissolved organic matter; PP, primary production.

non-cyanobacterial species. Thus, POC export was likely supported by diazotrophs, as observed *in-situ* (Bonnet et al., 2023), and cyanobacteria, as larger non-diazotroph phytoplankton developed belatedly and were still in exponential phase when the experiment was stopped. This suggests that the effect of fluids on POC export was likely underestimated in our experiment due to the limited incubation time considered.

5 Conclusion

This nine-day experiment demonstrates that, although hydrothermal fluids triggered an initial toxic effect on phytoplankton communities, these hydrothermal inputs ultimately stimulated NCP, N_2 fixation and POC export, in line with *in-situ* observations. This fertilizing effect occurred notably through rapid detoxification of the

potentially toxic trace metal-rich environment (a cocktail of trace metals such as Cu, Cd, Hg and Pb) by *Synechococcus* ecotypes, which are capable of producing organic ligands, such as thiols (TA- and GSH-like compounds) and FDOM (protein-like fluorophores). These ligands have been reported to significantly reduce the bioavailability of harmful elements to the planktonic communities and have probably allowed the environment to become suitable for the development of more sensitive communities (i.e., eukaryotes). Thus, species stressed by high concentrations of trace metals (haptophyceae, diatoms and dinoflagellates) were able to increase their growth rates, which were further enhanced by the supply of essential and fertilizing elements, especially Fe, by hydrothermal fluids (Figure 7). The experimental results are consistent with the *in-situ* observations performed during the TONGA expedition in the region impacted by hydrothermal fluids. They confirm the causal link between the supply of hydrothermal fluids into the photic layer, the intense biological productivity and the high rates of diazotrophy. This study highlights the implication of shallow hydrothermal systems as a trigger for high biological productivity in oligotrophic ocean areas. Such sources may be widespread in the global ocean and may have a significant impact on the functioning and effectiveness of the biological carbon pump.

This study revealed some shortcomings that need to be addressed in future experiments. Additional analyses of trace metal ionic concentrations in fluids from hydrothermal sources of the Tonga-Kermadec arc would have helped confirm the level of toxicity of metals triggering the production of thiols. A precise measurement of the dynamics of ionic forms of trace metals and their ligands during the experiment could be of great interest to better understand environmental detoxification. It would also be possible to repeat this experiment but over a longer time period to accurately estimate the effect of fluids on material export. Molecular analyses could also validate the hypothesis of the presence of resistant thiol-producing ecotypes of *Synechococcus* in hydrothermal fluids.

Data availability statement

The datasets presented in this study can be found in online repositories. The names of the repository/repositories and accession number(s) can be found below: http://www.obs-vlfr.fr/proof/php/TONGA/tonga.php.

Author contributions

FG and CéG designed the research. CT, EP-V, FG and CéG carried out the 9-day experiment in minicosms. CT conditioned HPLC samples. DM performed flow cytometry analyses, SB, MB, and CL measured the N_2 fixation, CT analyzed the nitrate, NCP, A_T and DFe samples, NL and CT analyzed the exported material, GP analyzed the thiol compounds, CaG and MT analyzed FDOM, EP-V analyzed DOP, M-EV analyzed pTM and FG analyzed pH_T. CT analyzed the data with the help of CéG and FG. The original draft was written by CT, CéG, and FG. All authors contributed to the article and approved the submitted version.

Funding

This work was performed in the framework of the TONGA project (TONGA cruise GEOTRACES GPpr14, November 2019, https://doi.org/10.17600/18000884) managed by the LOV (CéG) and the MIO (SB). The project was funded by the TGIR Flotte Océanographique Française, the A-MIDeX of Aix-Marseille University, the LEFE-CYBER and GMMC program and the Agence Nationale de Recherche (ANR-18-CE01-0016). GP was supported by a Natural Environment Research Council Doctoral Training Scholarship (NE/L002469/1).

Acknowledgments

We warmly thank all the scientists, the captain and the crew of the R/V l'Atalante for their cooperative work at sea. We especially thank all the individuals involved in the minicosm experiment for their great contribution to its success. We thank Céline Dimier and the SAPIGH platform of the Institut de la Mer de Villefranche (IMEV) for performing the pigment analyzes. We thank Sandra Nunige for the nutrient analyses. We warmly thank Matthieu Bressac, Veronica Arnone and David González-Santana for collecting dissolved and particulate metal end-member samples during the cruise. We thank Hélène Planquette for the analysis of the particulate trace metal end-member samples and for her review of the manuscript.

Conflict of interest

The authors declare that the research was conducted in the absence of any commercial or financial relationships that could be construed as a potential conflict of interest.

The handling editor IB-F is currently organizing a Research Topic with the authors SB and CG.

Publisher's note

Supplementary material

The Supplementary Material for this article can be found online at: https://www.frontiersin.org/articles/10.3389/fmars.2023.1082077/full#supplementary-material

References

Ahner, B. A., Lee, J. G., Price, N. M., and Morel, F. M. M. (1998). Phytochelatin concentrations in the equatorial pacific. *Deep Sea Res. Part I: Oceanog. Res. Pap.* 45, 1779–1796. doi: 10.1016/S0967-0637(98)00043-0

Ahner, B. A., and Morel, F. M. M. (1995). Phytochelatin production in marine algae. 2. induction by various metals. *Limnol. Oceanogr.* 40, 658–665. doi: 10.4319/lo.1995.40.4.0658

Ahner, B. A., Price, N. M., and Morel, F. M. (1994). Phytochelatin production by marine phytoplankton at low free metal ion concentrations: laboratory studies and field data from Massachusetts bay. *Proc. Natl. Acad. Sci. U.S.A.* 91, 8433–8436. doi: 10.1073/pnas.91.18.8433

Aiken, G. R. (2014). "Fluorescence and dissolved organic matter: A chemist's perspective., in: Aquatic organic matter fluorescence,". Eds. P. G. Coble, J. Lead, A. Baker, D. M. Reynolds and R. G. M. Spencer (New York, NY, USA: Cambridge University Press), 35–74. doi: 10.1017/CBO9781139045452

Ain Zainuddin, N., Azwan Raja Mamat, T., Imam Maarof, H., Wahidah Puasa, S., and Rohana Mohd Yatim, S. (2019). Removal of nickel, zinc and copper from plating process industrial raw effluent *Via* hydroxide precipitation versus sulphide precipitation. *IOP Conf. Ser.: Mater. Sci. Eng.* 551, 12122. doi: 10.1088/1757-899X/551/1/012122

Anderson, D. M., and Morel, F. M. M. (1978). Copper sensitivity of gonyaulax tamarensis 1: Cooper sensitivity. *Limnol. Oceanogr.* 23, 283–295. doi: 10.4319/lo.1978.23.2.0283

Ardyna, M., Lacour, L., Sergi, S., d'Ovidio, F., Sallée, J.-B., Rembauville, M., et al. (2019). Hydrothermal vents trigger massive phytoplankton blooms in the southern ocean. *Nat. Commun* 10, 1–8. doi: 10.1038/s41467-019-09973-6

Azeh Engwa, G., Udoka Ferdinand, P., Nweke Nwalo, F., and N. Unachukwu, M. (2019). "Mechanism and health effects of heavy metal toxicity in humans," in *Poisoning in the modern world - new tricks for an old dog*. Eds. O. Karcioglu and B. Arslan (Kazimierz Dolny, Poland: IntechOpen). doi: 10.5772/intechopen.82511

Behrenfeld, M. J., and Milligan, A. J. (2013). Photophysiological expressions of iron stress in phytoplankton. *Annu. Rev. Mar. Sci.* 5, 217–246. doi: 10.1146/annurev-marine-121211-172356

Benavides, M., Berthelot, H., Duhamel, S., Raimbault, P., and Bonnet, S. (2017). Dissolved organic matter uptake by trichodesmium in the southwest pacific. *Sci. Rep.* 7, 41315. doi: 10.1038/srep41315

Berman-Frank, I., Cullen, J. T., Shaked, Y., Sherrell, R. M., and Falkowski, P. G. (2001). Iron availability, cellular iron quotas, and nitrogen fixation in *Trichodesmium*. limnol. *Oceanogr* 46, 1249–1260. doi: 10.4319/lo.2001.46.6.1249

Berthelot, H., Bonnet, S., Grosso, O., Cornet, V., and Barani, A. (2016). Transfer of diazotroph-derived nitrogen towards non-diazotrophicplanktonic communities: a comparative study between<i<Trichodesmium</i< <i<erythraeum</i<, <i<Crocosphaerawatsonii</i< and <i<Cyanothece</i< sp. *Biogeosciences* 13, 4005–4021. doi: 10.5194/bg-13-4005-2016

Bonnet, S., Benavides, M., Le Moigne, F. A. C., Camps, M., Torremocha, A., Grosso, O., et al. (2023). Diazotrophs are overlooked contributors to carbon and nitrogen export to the deep ocean. *ISME J.* 17, 47–58. doi: 10.1038/s41396-022-01319-3

Bonnet, S., Caffin, M., Berthelot, H., Grosso, O., Benavides, M., Helias-Nunige, S., et al. (2018). In-depth characterization of diazotroph activity across the western tropical south pacific hotspot of N<sub<2</sub< fixation (OUTPACE cruise). *Biogeosciences* 15, 4215–4232. doi: 10.5194/bg-15-4215-2018

Bonnet, S., Caffin, M., Berthelot, H., and Moutin, T. (2017). Hot spot of n $_2$ fixation in the western tropical south pacific pleads for a spatial decoupling between n $_2$ fixation and denitrification. *Proc. Natl. Acad. Sci. U.S.A.* 114, E2800–E2801. doi: 10.1073/pnas.1619514114

Bonnet, S., Guieu, C., Taillandier, V., Boulart, C., Bouruet-Aubertot, P. , Gazeau, F., et al. (in rev). Natural iron fertilization by shallow hydrothermal sources fuels diazotroph blooms in the ocean. *Science*.

Brand, L. E., Sunda, W. G., and Guillard, R. R. L. (1986). Reduction of marine phytoplankton reproduction rates by copper and cadmium. *J. Exp. Mar. Biol. Ecol.* 96, 225–250. doi: 10.1016/0022-0981(86)90205-4

Brown, A. C., and Gordon, A. S. (2001). Production of a novel copper-binding ligand by marine synechococcus (Cyanobacteria) in response to toxic concentrations of copper. *Virginia J. Sci.* 52. doi: 10.25778/3Z1J-A974

Browning, T. J., Achterberg, E. P., Yong, J. C., Rapp, I., Utermann, C., Engel, A., et al. (2017). Iron limitation of microbial phosphorus acquisition in the tropical north Atlantic. *Nat. Commun.* 8, 15465. doi: 10.1038/ncomms15465

Buckberry, L. D., and Teesdale-Spittle, P. H. (1996). *Sulfur–hydrogen compounds, in: Biological interactions of sulfur compounds* Vol. p (London, UK ; Bristol, PA, USA: Taylor & Francis), 32.

Chen, W. B., Smith, D. S., and Guéguen, C. (2013). Influence of water chemistry and dissolved organic matter (DOM) molecular size on copper and mercury binding determined by multiresponse fluorescence quenching. *Chemosphere* 92, 351–359. doi: 10.1016/j.chemosphere.2012.12.075

Cobbett, C. S. (2000). Phytochelatins and their roles in heavy metal detoxification. *Plant Physiol.* 123, 825–832. doi: 10.1104/pp.123.3.825

Coble, P. G. (2007). Marine optical biogeochemistry: The chemistry of ocean color. *Chem. Rev.* 107, 402–418. doi: 10.1021/cr050350+

Coppellotti, O. (1989). Glutathione, cysteine and acid-soluble thiol levels in euglena gracilis cells exposed to copper and cadmium. *Comp. Biochem. Physiol. Part C: Comp. Pharmacol.* 94, 35–40. doi: 10.1016/0742-8413(89)90140-0

Corbett, C. (2007). *Colored dissolved organic matter (CDOM) workshop summary report*.

Croot, P. L., Moffett, J. W., and Brand, L. E. (2000). Production of extracellular Cu complexing ligands by eucaryotic phytoplankton in response to Cu stress. *Limnol. Oceanogr.* 45, 619–627. doi: 10.4319/lo.2000.45.3.0619

DalCorso, G. (2012). "Heavy metal toxicity in plants," in *Plants and heavy metals, SpringerBriefs in molecular science*. Ed. A. Furini (Netherlands, Dordrecht: Springer), 1–25. doi: 10.1007/978-94-007-4441-7_1

de Kluijver, A., Soetaert, K., Schulz, K. G., Riebesell, U., Bellerby, R. G. J., and Middelburg, J. J. (2010). Phytoplankton-bacteria coupling under elevated CO_2 levels: a stable isotope labelling study. *Biogeosciences* 7, 3783–3797. doi: 10.5194/bg-7-3783-2010

De Vos, C. H. R., Vonk, M. J., Vooijs, R., and Schat, H. (1992). Glutathione depletion due to copper-induced phytochelatin synthesis causes oxidative stress in *Silene cucubalus*. *Plant Physiol.* 98, 853–858. doi: 10.1104/pp.98.3.853

Dick, G. J., Anantharaman, K., Baker, B. J., Li, M., Reed, D. C., and Sheik, C. S. (2013). The microbiology of deep-sea hydrothermal vent plumes: ecological and biogeographic linkages to seafloor and water column habitats. *Front. Microbiol.* 4. doi: 10.3389/fmicb.2013.00124

Dupont, C. L., and Ahner, B. A. (2005). Effects of copper, cadmium, and zinc on the production and exudation of thiols by *Emiliania huxleyi*. limnol. *Oceanogr* 50, 508–515. doi: 10.4319/lo.2005.50.2.0508

Dupont, C. L., Moffett, J., Bidigare, R. R., and Ahner, B. A. (2006). Distributions of dissolved and particulate biogenic thiols in the subartic pacific ocean. *Deep Sea Res. Part I: Oceanog. Res. Pap.* 53, 1961–1974. doi: 10.1016/j.dsr.2006.09.003

Dyhrman, S. T., Chappell, P. D., Haley, S. T., Moffett, J. W., Orchard, E. D., Waterbury, J. B., et al. (2006). Phosphonate utilization by the globally important marine diazotroph trichodesmium. *Nature* 439, 68–71. doi: 10.1038/nature04203

Dyhrman, S. T., and Haley, S. T. (2006). Phosphorus scavenging in the unicellular marine diazotroph *Crocosphaera watsonii*. *Appl. Environ. Microbiol.* 72, 1452–1458. doi: 10.1128/AEM.72.2.1452-1458.2006

Echeveste, P., Agustí, S., and Tovar-Sánchez, A. (2012). Toxic thresholds of cadmium and lead to oceanic phytoplankton: Cell size and ocean basin-dependent effects. *Environ. Toxicol. Chem.* 31, 1887–1894. doi: 10.1002/etc.1893

Fernández-Juárez, V., Bennasar-Figueras, A., Tovar-Sanchez, A., and Agawin, N. S. R. (2019). The role of iron in the p-acquisition mechanisms of the unicellular N2-fixing cyanobacteria halothece sp., found in association with the Mediterranean seagrass posidonia oceanica. *Front. Microbiol.* 10. doi: 10.3389/fmicb.2019.01903

Ferretto, N., Tedetti, M., Guigue, C., Mounier, S., Raimbault, P., and Goutx, M. (2017). Spatio-temporal variability of fluorescent dissolved organic matter in the rhône river delta and the fos-marseille marine area (NW Mediterranean Sea, France). *Environ. Sci. pollut. Res.* 24, 4973–4989. doi: 10.1007/s11356-016-8255-z

German, C. R., Casciotti, K. A., Dutay, J.-C., Heimbürger, L. E., Jenkins, W. J., Measures, C. I., et al. (2016). Hydrothermal impacts on trace element and isotope ocean biogeochemistry. *Philos. Trans. R. Soc. A: Math. Phys. Eng. Sci.* 374, 20160035. doi: 10.1098/rsta.2016.0035

Gharabaghi, M., Irannajad, M., and Azadmehr, A. R. (2012). Selective sulphide precipitation of heavy metals from acidic polymetallic aqueous solution by thioacetamide. *Ind. Eng. Chem. Res.* 51, 954–963. doi: 10.1021/ie201832x

González-Vega, A., Fraile-Nuez, E., Santana-Casiano, J. M., González-Dávila, M., Escánez-Pérez, J., Gómez-Ballesteros, M., et al. (2020). Significant release of dissolved inorganic nutrients from the shallow submarine volcano tagoro (Canary islands) based on seven-year monitoring. *Front. Mar. Sci.* 6. doi: 10.3389/fmars.2019.00829

Grill, E., Löffler, S., Winnacker, E.-L., and Zenk, M. H. (1989). Phytochelatins, the heavy-metal-binding peptides of plants, are synthesized from glutathione by a specific γ-glutamylcysteine dipeptidyl transpeptidase (phytochelatin synthase). *Proc. Natl. Acad. Sci. U.S.A.* 86, 6838–6842. doi: 10.1073/pnas.86.18.6838

Guieu, C., and Bonnet, S. (2019). *TONGA cruise 2019, L'Atalante R/V*. doi: 10.17600/18000884

Guieu, C., Bonnet, S., Petrenko, A., Menkes, C., Chavagnac, V., Desboeufs, K., et al. (2018). Iron from a submarine source impacts the productive layer of the Western tropical south pacific (WTSP). *Sci. Rep.* 8, 1–9. doi: 10.1038/s41598-018-27407-z

Hawkes, J. A., Connelly, D. P., Rijkenberg, M. J. A., and Achterberg, E. P. (2014). The importance of shallow hydrothermal island arc systems in ocean biogeochemistry. *Geophys. Res. Lett.* 41, 942–947. doi: 10.1002/2013GL058817

Hoffmann, L. J., Breitbarth, E., Ardelan, M. V., Duggen, S., Olgun, N., Hassellöv, M., et al. (2012). Influence of trace metal release from volcanic ash on growth of thalassiosira pseudonana and emiliania huxleyi. *Mar. Chem.* 132–133, 28–33. doi: 10.1016/j.marchem.2012.02.003

Horvatić, J., and Peršić, V. (2007). The effect of Ni2+, Co2+, Zn2+, Cd2+ and Hg2+ on the growth rate of marine diatom phaeodactylum tricornutum bohlin: Microplate growth inhibition test. *Bull. Environ. Contam Toxicol.* 79, 494–498. doi: 10.1007/s00128-007-9291-7

Huckle, J. W., Morby, A. P., Turner, J. S., and Robinson, N. J. (1993). Isolation of a prokaryotic metallothionein locus and analysis of transcriptional control by trace metal ions. *Mol. Microbiol.* 7, 177–187. doi: 10.1111/j.1365-2958.1993.tb01109.x

James, G., Witten, D., Hastie, T., and Tibshirani, R. (2013). *An introduction to statistical learning, springer texts in statistics* (New York, NY: Springer New York). doi: 10.1007/978-1-4614-7138-7

Joux-Arab, L., Berthet, B., and Robert, J.-M. (2000). Do toxicity and accumulation of copper change during size reduction in the marine pennate diatom haslea ostrearia? *Mar. Biol.* 136, 323–330. doi: 10.1007/s002270050690

Klawonn, I., Lavik, G., Böning, P., Marchant, H. K., Dekaezemacker, J., Mohr, W., et al. (2015). Simple approach for the preparation of 15–15N2-enriched water for nitrogen fixation assessments: evaluation, application and recommendations. *Front. Microbiol.* 6. doi: 10.3389/fmicb.2015.00769

Lage, O. M., Parente, A. M., Soares, H. M. V. M., Vasconcelos, M. T. S. D., and Salema, R. (1994). Some effects of copper on the dinoflagellates *Amphidinium carterae* and *Prorocentrum micans* in batch culture. *Eur. J. Phycol.* 29, 253–260. doi: 10.1080/09670269400650711

Lage, O. M., Sansonetty, F., O'Connor, J.-E., and Parente, A. M. (2001). Flow cytometric analysis of chronic and acute toxicity of copper(II) on the marine dinoflagellateAmphidinium carterae. *Cytometry* 44, 226–235. doi: 10.1002/1097-0320(20010701)44:3<226::AID-CYTO1115>3.0.CO;2-9

Lage, O. M., Soares, H. M. V. M., Vasconcelos, M. T. S. D., Parente, A. M., and Salema, R. (1996). Toxicity effects of copper (II) on the marine dinoflagellate *Amphidinium carterae* : Influence of metal speciation. *Eur. J. Phycol.* 31, 341–348. doi: 10.1080/09670269600651571

Lavigne, H., and Gattuso, J.-P. (2010). *Seacarb: seawater carbonate chemistry with r*.

Leal, M. F. C., Vasconcelos, M. T. S. D., and van den Berg, C. M. G. (1999). Copper-induced release of complexing ligands similar to thiols by emiliania huxleyi inseawater cultures. *Limnol. Oceanogr.* 44, 1750–1762. doi: 10.4319/lo.1999.44.7.1750

Le Faucheur, S., Campbell, P. G. C., Fortin, C., and Slaveykova, V. I. (2014). Interactions between mercury and phytoplankton: Speciation, bioavailability, and internal handling: Mercury-phytoplankton interactions. *Environ. Toxicol. Chem.* 33, 1211–1224. doi: 10.1002/etc.2424

Le Gall, C., and Van Den Berg, C. M. G. (1998). Folic acid and glutathione in the water column of the north East Atlantic. *Deep Sea Res. Part I: Oceanog. Res. Pap.* 45, 1903–1918. doi: 10.1016/S0967-0637(98)00042-9

Le Jeune, A.-H., Charpin, M., Deluchat, V., Briand, J.-F., Lenain, J.-F., Baudu, M., et al. (2006). Effect of copper sulphate treatment on natural phytoplanktonic communities. *Aquat. Toxicol* 80, 267–280. doi: 10.1016/j.aquatox.2006.09.004

Lenth, R., Singmann, H., Love, J., Buerkner, P., and Herve, M. (2019). *Package "emmeans"*.

Levy, J. L., Stauber, J. L., and Jolley, D. F. (2007). Sensitivity of marine microalgae to copper: The effect of biotic factors on copper adsorption and toxicity. *Sci. Total Environ.* 387, 141–154. doi: 10.1016/j.scitotenv.2007.07.016

Liang, Z., Letscher, R. T., and Knapp, A. N. (2022). Dissolved organic phosphorus concentrations in the surface ocean controlled by both phosphate and iron stress. *Nat. Geosci.* 15, 651–657. doi: 10.1038/s41561-022-00988-1

Lilley, M. D., Feely, R. A., and Trefry, J. H. (2013). Chemical and biochemical transformations in hydrothermal plumes, in: Seafloor hydrothermal systems: Physical, chemical, biological, and geological interactions. *Am. Geophys. Union (AGU)* pp, 369–391. doi: 10.1029/GM091p0369

Liu, J., Zhou, L., Ke, Z., Li, G., Shi, R., and Tan, Y. (2018). Beneficial effects of aluminum enrichment on nitrogen-fixing cyanobacteria in the south China Sea. *Mar. pollut. Bull.* 129, 142–150. doi: 10.1016/j.marpolbul.2018.02.011

Lory, C., Van Wambeke, F., Fourquez, M., Berman-Frank, I., Barani, A., Tilliette, C., et al. (2022). Assessing the contribution of diazotrophs to microbial fe uptake using a group specific approach in the Western tropical south pacific ocean. *ISME Commun.* doi: 10.1038/s43705-022-00122-7

Lou, Y., He, Z., and Han, X. (2020). Transport and deposition patterns of particles laden by rising submarine hydrothermal plumes. *Geophys. Res. Lett.* 47. doi: 10.1029/2020GL089935

Mann, E. L., Ahlgren, N., Moffett, J. W., and Chisholm, S. W. (2002). Copper toxicity and cyanobacteria ecology in the Sargasso Sea. *Limnol. Oceanogr.* 47, 976–988. doi: 10.4319/lo.2002.47.4.0976

Marie, D., Partensky, F., Vaulot, D., and Brussaard, C. (1999). Enumeration of phytoplankton, bacteria, and viruses in marine samples. *Curr. Protoc. Cytomet.* 10. doi: 10.1002/0471142956.cy1111s10

Martin, J. H. (1990). Glacial-interglacial CO_2 change: The iron hypothesis. *Paleoceanography* 5, 1–13. doi: 10.1029/PA005i001p00001

Massoth, G., Baker, E., Worthington, T., Lupton, J., de Ronde, C., Arculus, R., et al. (2007). Multiple hydrothermal sources along the south Tonga arc and valu fa ridge. *Geochem. Geophys. Geosyst* 8. doi: 10.1029/2007GC001675

Maugendre, L., Gattuso, J.-P., de Kluijver, A., Soetaert, K., van Oevelen, D., Middelburg, J. J., et al. (2017). Carbon-13 labelling shows no effect of ocean acidification on carbon transfer in Mediterranean plankton communities. *Estuar. Coast. Shelf Sci.* 186, 100–111. doi: 10.1016/j.ecss.2015.12.018

May, M. J., Vernoux, T., Leaver, C., Montagu, M. V., and Inze, D. (1998). Glutathione homeostasis in plants: implications for environmental sensing and plant development. *J. Exp. Bot.* 49, 649–667. doi: 10.1093/jxb/49.321.649

Mehana, E.-S. (2014). Impact of water pollution with heavy metals on fish health:Overview and updates. *Global Veterinaria* 12, 219–231. doi: 10.5829/idosi.gv.2014.12.02.82219

Moffett, J. W., and Brand, L. E. (1996). Production of strong, extracellular Cu chelators by marine cyanobacteria in response to Cu stress. *Limnol. Oceanogr.* 41, 388–395. doi: 10.4319/lo.1996.41.3.0388

Moffett, J. W., Zika, R. G., and Brand, L. E. (1990). Distribution and potential sources and sinks of copper chelators in the Sargasso Sea. *Deep Sea Res. Part A. Oceanog. Res. Pap.* 37, 27–36. doi: 10.1016/0198-0149(90)90027-S

Moisander, P. H., Serros, T., Paerl, R. W., Beinart, R. A., and Zehr, J. P. (2014). Gammaproteobacterial diazotrophs and nifH gene expression in surface waters of the south pacific ocean. *ISME J.* 8, 1962–1973. doi: 10.1038/ismej.2014.49

Montoya, J. P., Voss, M., Kahler, P., and Capone, D. G. (1996). A simple, high-precision, high-sensitivity tracer assay for N(inf2) fixation. *Appl. Environ. Microbiol.* 62, 986–993. doi: 10.1128/aem.62.3.986-993.1996

Morel, F. M. M., and Price, N. M. (2003). The biogeochemical cycles of trace metals in the oceans. *Science* 300, 944–947. doi: 10.1126/science.1083545

Morrison, R. T., Boyd, R. N., and Bhattacharjee, S. K. (2010). *Organic chemistry*.

Mounier, S., Zhao, H., Garnier, C., and Redon, R. (2011). Copper complexing properties of dissolved organic matter: PARAFAC treatment of fluorescence quenching. *Biogeochemistry* 106, 107–116. doi: 10.1007/s10533-010-9486-6

Moutin, T., and Bonnet, S. (2015). *OUTPACE cruise,L'Atalante R/V*. doi: 10.17600/15000900

Moutin, T., Karl, D. M., Duhamel, S., Rimmelin, P., Raimbault, P., Van Mooy, B. A. S., et al. (2008). Phosphate availability and the ultimate control of new nitrogen input by nitrogen fixation in the tropical pacific ocean. *Biogeosciences* 5, 95–109. doi: 10.5194/bg-5-95-2008

Moutin, T., Van Den B, B., Beker, B., Dupouy, C., Rimmelin, P., and Le Bouteiller, A. (2005). Phosphate availability controls trichodesmium spp. *Biomass SW Pacific Ocean. Mar. Ecol. Prog. Ser.* 297, 15–21. doi: 10.3354/meps297015

Mujika, J. I., Ruipérez, F., Infante, I., Ugalde, J. M., Exley, C., and Lopez, X. (2011). Pro-oxidant activity of aluminum: Stabilization of the aluminum superoxide radical ion. *J. Phys. Chem. A* 115, 6717–6723. doi: 10.1021/jp203290b

Noctor, G., Arisi, A.-C. M., Jouanin, L., Kunert, K. J., Rennenberg, H., and Foyer, C. H. (1998). Glutathione: biosynthesis, metabolism and relationship to stress tolerance explored in transformed plants. *J. Exp. Bot.* 49, 623–647. doi: 10.1093/jxb/49.321.623

Okamoto, O. K., Shao, L., Woodland Hastings, J., and Colepicolo, P. (1999). Acute and chronic effects of toxic metals on viability, encystment and bioluminescence in the dinoflagellate gonyaulax polyedra. *Comp. Biochem. Physiol. Part C: Pharmacol. Toxicol. Endocrinol.* 123, 75–83. doi: 10.1016/S0742-8413(99)00013-4

Omanović, D., and Branica, M. (1998). Automation of voltammetric measurements by polarographic analyser PAR 384B. *Croatica Chemica Acta* 71, 421–433.

Palenik, B., Ren, Q., Dupont, C. L., Myers, G. S., Heidelberg, J. F., Badger, J. H., et al. (2006). Genome sequence of *Synechococcus* CC9311: Insights into adaptation to a coastal environment. *Proc. Natl. Acad. Sci. U.S.A.* 103, 13555–13559. doi: 10.1073/pnas.0602963103

Pelletier, B., Calmant, S., and Pillet, R. (1998). Current tectonics of the Tonga–new Hebrides region. *Earth Planet. Sci. Lett.* 164, 263–276. doi: 10.1016/S0012-821X(98)00212-X

Permana, R., and Akbarsyah, N. (2021). Phytoplankton susceptibility towards toxic heavy metal cadmium: Mechanism and its recent updates. *World News Natural Sci.* 38, 83–97.

Pernet-Coudrier, B., Waeles, M., Filella, M., Quentel, F., and Riso, R. D. (2013). Simple and simultaneous determination of glutathione, thioacetamide and refractory organic matter in natural waters by DP-CSV. *Sci. Total Environ.* 463–464, 997–1005. doi: 10.1016/j.scitotenv.2013.06.053

Pinto, E., Sigaud-kutner, T. C. S., Leitao, M. A. S., Okamoto, O. K., Morse, D., and Colepicolo, P. (2003). Heavy metal-induced oxidative stress in algae. *J. Phycol* 39, 1008–1018. doi: 10.1111/j.0022-3646.2003.02-193.x

Pollard, R., Sanders, R., Lucas, M., and Statham, P. (2007). The crozet natural iron bloom and export experiment (CROZEX). *Deep Sea Res. Part II: Top. Stud. Oceanog.* 54, 1905–1914. doi: 10.1016/j.dsr2.2007.07.023

Quigg, A., Reinfelder, J. R., and Fisher, N. S. (2006). Copper uptake kinetics in diverse marine phytoplankton. *Limnol. Oceanogr.* 51, 893–899. doi: 10.4319/lo.2006.51.2.0893

Raven, J. A. (1988). The iron and molybdenum use efficiencies of plant growth with different energy, carbon and nitrogen sources. *New Phytol.* 109, 279–287. doi: 10.1111/j.1469-8137.1988.tb04196.x

Rijstenbil, J. W., Derksen, J. W. M., Gerringa, L. J. A., Poortvliet, T. C. W., Sandee, A., van den Berg, M., et al. (1994). Oxidative stress induced by copper: defense and damage in the marine planktonic diatom ditylum brightwellii, grown in continuous cultures with high and low zinc levels. *Mar. Biol.* 119, 583–590. doi: 10.1007/BF00354321

Rinard Hinga, B. D. (2015). *Ring of fire: an encyclopedia of the pacific rim's earthquakes, tsunamis, and volcanoes* (Santa Barbara, California: ABC-CLIO).

Romano, R. L., Liria, C. W., Machini, M. T., Colepicolo, P., and Zambotti-Villela, L. (2017). Cadmium decreases the levels of glutathione and enhances the phytochelatin concentration in the marine dinoflagellate lingulodinium polyedrum. *J. Appl. Phycol* 29, 811–820. doi: 10.1007/s10811-016-0927-z

Rueter, J. G., Hutchins, D. A., Smith, R. W., and Unsworth, N. L. (1992). "Iron nutrition of trichodesmium," in *Marine pelagic cyanobacteria: Trichodesmium and other diazotrophs*. Eds. E. J. Carpenter, D. G. Capone and J. G. Rueter (Netherlands, Dordrecht: Springer), 289–306. doi: 10.1007/978-94-015-7977-3_19

Ruipérez, F., Mujika, J. I., Ugalde, J. M., Exley, C., and Lopez, X. (2012). Pro-oxidant activity of aluminum: Promoting the fenton reaction by reducing Fe(III) to Fe(II). *J. Inorganic Biochem.* 117, 118–123. doi: 10.1016/j.jinorgbio.2012.09.008

Satoh, M., Hirachi, Y., Yoshioka, A., Kobayashi, M., and Oyama, Y. (2002). Determination of cellular levels of nonprotein thiols in phytoplankton and their correlations with susceptibility to mercury. *J. Phycol* 38, 983–990. doi: 10.1046/j.1529-8817.2002.t01-1-01223.x

Satoh, M., Karaki, E., Kakehashi, M., Okazaki, E., Gotoh, T., and Oyama, Y. (1999). Heavy-metal induced changes in nonproteinaceous thiol levels and heavy-metal binding peptide in tetraselmis tetrathele (Prasinophyceae). *J. Phycol* 35, 989–994. doi: 10.1046/j.1529-8817.1999.3550989.x

Scheller, H. V., Huang, B., Hatch, E., and Goldsbrough, P. B. (1987). Phytochelatin synthesis and glutathione levels in response to heavy metals in tomato cells. *Plant Physiol.* 85, 1031–1035. doi: 10.1104/pp.85.4.1031

Schine, C. M. S., Alderkamp, A.-C., van Dijken, G., Gerringa, L. J. A., Sergi, S., Laan, P., et al. (2021). Massive southern ocean phytoplankton bloom fed by iron of possible hydrothermal origin. *Nat. Commun.* 12, 1211. doi: 10.1038/s41467-021-21339-5

Schlitzer, R., Anderson, R. F., Dodas, E. M., Lohan, M., Geibert, W., Tagliabue, A., et al. (2018). The GEOTRACES intermediate data product 2017. *Chem. Geol.* 493, 210–223. doi: 10.1016/j.chemgeo.2018.05.040

Schlosser, C., Klar, J. K., Wake, B. D., Snow, J. T., Honey, D. J., Woodward, E. M. S., et al. (2014). Seasonal ITCZ migration dynamically controls the location of the (sub) tropical Atlantic biogeochemical divide. *Proc. Natl. Acad. Sci. U.S.A.* 111, 1438–1442. doi: 10.1073/pnas.1318670111

Shaked, Y., Kustka, A. B., and Morel, F. M. M. (2005). A general kinetic model for iron acquisition by eukaryotic phytoplankton. *Limnol. Oceanogr.* 50, 872–882. doi: 10.4319/lo.2005.50.3.0872

Stauber, J. L., and Davies, C. M. (2000). Use and limitations of microbial bioassays for assessing copper bioavailability in the aquatic environment. *Environ. Rev.* 8, 255–301. doi: 10.1139/a00-010

Stedmon, C. A., and Bro, R. (2008). Characterizing dissolved organic matter fluorescence with parallel factor analysis: a tutorial: Fluorescence-PARAFAC analysis of DOM. *Limnol. Oceanogr. Methods* 6, 572–579. doi: 10.4319/lom.2008.6.572

Stuart, R. K., Brahamsha, B., Busby, K., and Palenik, B. (2013). Genomic island genes in a coastal marine synechococcus strain confer enhanced tolerance to copper and oxidative stress. *ISME J.* 7, 1139–1149. doi: 10.1038/ismej.2012.175

Stuart, R. K., Dupont, C. L., Johnson, D. A., Paulsen, I. T., and Palenik, B. (2009). Coastal strains of marine *Synechococcus* species exhibit increased tolerance to copper shock and a distinctive transcriptional response relative to those of open-ocean strains. *Appl. Environ. Microbiol.* 75, 5047–5057. doi: 10.1128/AEM.00271-09

Sunda, W. G. (1994). "Trace Metal/Phytoplankton interactions in the Sea," in *Chemistry of aquatic systems: Local and global perspectives*. Eds. G. Bidoglio and W. Stumm (Netherlands, Dordrecht: Springer), 213–247. doi: 10.1007/978-94-017-1024-4_9

Sunda, W. G., and Huntsman, S. A. (1995). Iron uptake and growth limitation in oceanic and coastal phytoplankton. *Mar. Chem.* 50, 189–206. doi: 10.1016/0304-4203(95)00035-P

Sunda, W. G., and Huntsman, S. A. (1998). Interactive effects of external manganese, the toxic metals copper and zinc, and light incontrolling cellular manganese and growth in a coastal diatom. *Limnol. Oceanogr.* 43, 1467–1475. doi: 10.4319/lo.1998.43.7.1467

Tagliabue, A., Bopp, L., Dutay, J.-C., Bowie, A. R., Chever, F., Jean-Baptiste, P., et al. (2010). Hydrothermal contribution to the oceanic dissolved iron inventory. *Nat. Geosci.* 3, 252–256. doi: 10.1038/ngeo818

Tang, D., Hung, C.-C., Warnken, K. W., and Santschi, P. H. (2000). The distribution of biogenic thiols in surface waters of Galveston bay. *Limnol. Oceanogr.* 45, 1289–1297. doi: 10.4319/lo.2000.45.6.1289

F. J. R. Taylor (Ed.) (1987). "The biology of dinoflagellates," in *Botanical monographs* (Oxford ; Boston: Blackwell Scientific Publications).

Tedetti, M., Bigot, L., Turquet, J., Guigue, C., Ferretto, N., Goutx, M., et al. (2020). Influence of freshwater discharges on biogeochemistry and benthic communities of a coral reef ecosystem (La réunion island, Indian ocean). *Front. Mar. Sci.* 7. doi: 10.3389/fmars.2020.596165

Tedetti, M., Marie, L., Röttgers, R., Rodier, M., Van Wambeke, F., Helias, S., et al. (2016). Evolution of dissolved and particulate chromophoric materials during the VAHINE mesocosm experiment in the new caledonian coral lagoon (south-west pacific). *Biogeosciences* 13, 3283–3303. doi: 10.5194/bg-13-3283-2016

Thomas, W. H., Hollibaughl, J. T., Seibertl, D. L. R., and Wallace, G. T. (1980). Toxicity of a mixture of ten metals to phytoplankton. *Mar. Ecol. Prog. Ser.* 2, 213–220. doi: 10.3354/meps002213

Tilliette, C., Taillandier, V., Bouruet-Aubertot, P., Grima, N., Maes, C., Montanes, M., et al. (2022). Dissolved iron patterns impacted by shallow hydrothermal sources along a transect through the Tonga-kermadec arc. *Global Biogeochem. Cycles*. doi: 10.1029/2022GB007363

Timm, C., Bassett, D., Graham, I. J., Leybourne, M. I., de Ronde, C. E. J., Woodhead, J., et al. (2013). Louisville Seamount subduction and its implication on mantle flow beneath the central Tonga–kermadec arc. *Nat. Commun.* 4, 1720. doi: 10.1038/ncomms2702

Uitz, J., Claustre, H., Morel, A., and Hooker, S. B. (2006). Vertical distribution of phytoplankton communities in open ocean: An assessment based on surface chlorophyll. *J. Geophys. Res.: Oceans* 111. doi: 10.1029/2005JC003207

Valsami-Jones, E., Baltatzis, E., Bailey, E. H., Boyce, A. J., Alexander, J. L., Magganas, A., et al. (2005). The geochemistry of fluids from an active shallow submarine hydrothermal system: Milos island, Hellenic volcanic arc. *J. Volcanol. Geothermal Res.* 148, 130–151. doi: 10.1016/j.jvolgeores.2005.03.018

Walker, S. L., and Baker, E. T. (1988). Particle-size distributions within hydrothermal plumes over the Juan de fuca ridge. *Mar. Geol.* 78, 217–226. doi: 10.1016/0025-3227(88)90110-7

Walsh, M. J., Goodnow, S. D., Vezeau, G. E., Richter, L. V., and Ahner, B. A. (2015). Cysteine enhances bioavailability of copper to marine phytoplankton. *Environ. Sci. Technol.* 49, 12145–12152. doi: 10.1021/acs.est.5b02112

Wong, K. H., Obata, H., Kim, T., Wakuta, Y., and Takeda, S. (2019). Distribution and speciation of copper and its relationship with FDOM in the East China Sea. *Mar. Chem.* 212, 96–107. doi: 10.1016/j.marchem.2019.04.005

Worms, I., Simon, D. F., Hassler, C. S., and Wilkinson, K. J. (2006). Bioavailability of trace metals to aquatic microorganisms: importance of chemical, biological and physical processes on biouptake. *Biochimie* 88, 1721–1731. doi: 10.1016/j.biochi.2006.09.008

Wu, Y., and Wang, W.-X. (2011). Accumulation, subcellular distribution and toxicity of inorganic mercury and methylmercury in marine phytoplankton. *Environ. pollut.* 159, 3097–3105. doi: 10.1016/j.envpol.2011.04.012

Wu, Y., and Wang, W.-X. (2012). Thiol compounds induction kinetics in marine phytoplankton during and after mercury exposure. *J. Haz. Mat.* 217–218, 271–278. doi: 10.1016/j.jhazmat.2012.03.024

Zenk, M. H. (1996). Heavy metal detoxification in higher plants - a review. *Gene* 179, 21–30. doi: 10.1016/S0378-1119(96)00422-2

Zhang, Z., Fan, W., Bao, W., Chen, C.-T. A., Liu, S., and Cai, Y. (2020). Recent developments of exploration and detection of shallow-water hydrothermal systems. *Sustainability* 12, 9109. doi: 10.3390/su12219109